https://doi.org/10.5194/egusphere-2026-1320
Preprint. Discussion started: 7 April 2026

Impact Comparison of Different Aerosol Types on Atmospheric Correction of Landsat 8 over Land

Shuning Zhang [1, 2, 3], Hao Zhang[4], Bing Zhang[3, 4], Zhenzhen Cui[1, 2]

[1]The Key Laboratory of Digital Earth Science, Aerospace Information Research Institute, Chinese Academy of Sciences, Beijing 100094, China;
[2]The International Research Center of Big Data for Sustainable Development Goals, Beijing 100094, China
[3]The College of Resources and Environment, University of Chinese Academy of Sciences, Beijing 100049, China
[4]The State Key Laboratory of Remote Sensing and Digital Earth, Aerospace Information Research Institute, Chinese Academy of Sciences, Beijing 100094, China

Correspondence to: Shuning Zhang (zhangshuning21@mails.ucas.ac.cn)

Abstract. The official Landsat 8 surface reflectance (SR) product, generated by the Land Surface Reflectance (LaSRC) algorithm, is the most extensively utilized medium-resolution dataset and serves as a benchmark to cross-validate the accuracy of other SR products. However, the accuracy of the Landsat 8 SR products did not meet the expectations of the previous studies under specific conditions. Consequently, it is necessary to analyze the Urban Clean aerosol-type assumption implemented in the LaSRC algorithm and comprehensively re-evaluate the accuracy of the Landsat 8 SR. Therefore, this study leverages Landsat 8 data over 600 scenes acquired at 100 Aerosol Robotic Network (AERONET) sites globally and conducts a comprehensive analysis of how different aerosol types—MOD04-based (used in the Moderate Resolution Imaging Spectroradiometer (MODIS) Atmosphere Level-2 Aerosol Optical Depth Product), MOD09-based (used in MODIS Terra Atmospherically Corrected Surface Reflectance Product), and Urban Clean (used in LaSRC)—affect the accuracy of atmospheric correction (AC) for the first time. The results indicated that, in terms of aerosol optical depth (AOD), the MOD04 aerosol type exhibited the highest accuracy, with an R^2 of 0.762, Root Mean Square Error (RMSE) of 0.0437, and bias of 0.0876. The accuracy, precision, and uncertainty of the SR products corresponding to the three aerosol types were within the ranges of 0.00036–0.00043, 0.02382–0.02468, and 0.02337–0.02425, respectively. The MOD04-based aerosol type demonstrated the highest overall accuracy in the visible and near-infrared (VNIR) bands. The MOD09-based aerosol type outperformed the others in the bright surface regions. The Urban Clean aerosol type showed a comparable but slightly inferior performance to that of the MOD09-based aerosol type, with limited advantages in specific reflectance ranges. Moreover, LaSRC-derived SR demonstrated higher stability and accuracy in the shortwave infrared (SWIR) bands compared to its inferior performance in the VNIR. These findings emphasize the critical importance of aerosol-type assumptions in AC workflow. A mixed strategic implementation framework is proposed as follows: (1) adopt MOD04-based aerosol types for AOD retrieval and VNIR SR retrieval, (2) utilize MOD09-based aerosol types to process data acquired over bright surface processing, and (3) leverage SWIR SR products derived by LaSRC. Our findings provide actionable guidelines for dynamic aerosol-type selection to enhance the AC performance across diverse environments.

https://doi.org/10.5194/egusphere-2026-1320
Preprint. Discussion started: 7 April 2026

1 Introduction

Atmospheric correction (AC), a critical component of remote sensing data processing, aims to mitigate atmospheric scattering and absorption effects on electromagnetic signals and convert sensor-received radiance into accurate surface reflectance (SR). Aerosols are key atmospheric constituents that significantly influence radiative transfer processes, cloud formation mechanisms, and atmospheric environmental dynamics (Dubovik et al., 2000; Levy et al., 2007a; Satheesh et al., 2005). Accurate aerosol parameter retrieval therefore plays a fundamental role in atmospheric remote sensing and directly governs AC performance (Zhang et al., 2009). Numerous aerosol optical depth (AOD) retrieval algorithms have been developed, among which physically based approaches remain the most widely adopted. Representative methods include the Dense Dark Vegetation algorithm (Kaufman et al., 1997) and the Deep Blue algorithm (Hsu et al., 2013). In recent years, multi-angle and multi-sensor retrieval strategies have further improved AOD estimation by enhancing surface–atmosphere separation and reducing uncertainties in SR assumptions. For example, the Multi-angle Implementation of Atmospheric Correction (MAIAC) algorithm developed for MODIS (Lyapustin et al., 2018) and MISR multi-angle retrievals combining nine viewing geometries have demonstrated improved performance, particularly over bright and heterogeneous surfaces (Chen et al., 2024). Meanwhile, data-driven approaches such as random forest, XGBoost, and deep neural networks have shown promising performance in capturing nonlinear relationships between atmospheric parameters and spectral observations (Radosavljevic et al., 2007). Recent studies have further incorporated temporal and spectral dependencies through advanced architectures, such as Transformer-based models applied to Himawari-8 time series data （She et al., 2024）, and multilayer aerosol retrieval integrating geostationary SEVIRI data with CALIOP vertical aerosol profiles (Pashayi et al., 2025). Despite these advances, data-driven and multi-sensor methods generally require extensive training datasets and complex model structures, and they often lack physical interpretability. Consequently, physically based algorithms remain the dominant approach in operational AC systems and serve as a standard reference for remote sensing applications. Within physically based AC frameworks, aerosol-type classification provides an efficient strategy to represent aerosol optical properties and improve retrieval adaptability. The development of aerosol classification has been greatly supported by globally distributed ground-based observation networks, including the Aerosol Robotic Network (AERONET) (Holben et al., 1998), the Sun–sky radiometer Observation Network (SONET) (Li et al., 2018), and SKYNET (Takamura et al., 2004). Early aerosol studies introduced simplified physical models with fixed parameters describing particle size distribution, chemical composition, and optical characteristics such as extinction coefficient, single scattering albedo, and phase function. Representative developments include lower-layer aerosol classifications proposed by Shettle et al. (Shettle et al., 1979), naval aerosol characterization by Gathman (Gathman et al., 1983), and desert aerosol models summarized by Longtin et al. (Longtin et al., 1988). Additionally, the World Meteorological Organization (WMO) identified representative aerosol categories including continental, maritime, urban, desert, biomass burning, and stratospheric aerosols in its reports (World Meteorological Organization, 1983; World Meteorological Organization, 1986). These fixed-parameter aerosol models remain essential components in radiative transfer models (RTMs), ensuring computational efficiency and stable

https://doi.org/10.5194/egusphere-2026-1320
Preprint. Discussion started: 7 April 2026

performance. For instance, the MODTRAN model includes predefined aerosol types such as rural, urban, maritime, and desert (Berk et al., 2018), while the 6S and vector 6SV models incorporate continental, urban, maritime, and desert aerosol models (Vermote et al., 1997). These classical aerosol representations have been widely applied in AC processing across diverse environmental conditions.

However, fixed-parameter aerosol models cannot fully capture the dynamic variability of atmospheric aerosols. To address this limitation, dynamic aerosol models, whose optical properties vary with AOD, have been developed based on global observational datasets. Since the 1990s, this research field has progressed significantly. Kaufman and Remer introduced fine-mode-dominated aerosol models such as urban/industrial and biomass burning/developing world aerosol types (Kaufman et al., 1997; Remer et al., 1998), while Ichoku et al. proposed highly absorbing aerosol models derived from African field observations (ECK et al., 2003; Ichoku et al., 2003). The integration of dynamic aerosol models provides more flexible and realistic atmospheric characterization and improves the adaptability of AC algorithms under diverse atmospheric conditions.

Through the integration of multiple aerosol models, AC algorithms have been continuously refined. Currently, fixed-parameter aerosol types remain dominant in operational AC processing. Commercial remote sensing software packages such as ATCOR (Richter et al., 2019), Atmospheric Correction Now (ACORN) (Miller et al., 2002), and Fast Line-of-sight Atmospheric Analysis of Hypercubes (FLAASH) (Anderson et al., 1999) rely on predefined aerosol types derived from MODTRAN to ensure efficient processing and reliable correction performance. Similarly, the Sentinel-2 atmospheric correction processor Sen2Cor adopts a fixed atmospheric model and supports four predefined aerosol types based on the libRadtran4 database (Anderson et al., 2012; Mueller-Wilm et al., 2017). Their continued application reflects a balance between physical reliability and computational efficiency, making them suitable for large-scale routine remote sensing applications.

Meanwhile, dynamic aerosol models have been increasingly incorporated into satellite AC algorithms. A representative example is the evolution of Landsat AC processing, which transitioned from fixed aerosol assumptions to dynamic aerosol modeling. The LEDAPS algorithm (Vermote et al., 2007) applied to Landsat TM/ETM+ sensors adopts a fixed continental aerosol type, whereas the Land Surface Reflectance Code (LaSRC) algorithm for Landsat 8 integrates the Urban Clean dynamic aerosol model (Dubovik et al., 2002; Maciel et al., 2023; Vermote et al., 2016). Similarly, MODIS AC algorithms employ dynamic combinations of coarse-mode dust and fine-mode aerosol components (Kaufman et al., 1997; Remer et al., 2005), and later incorporated highly absorbing aerosol types to better represent global atmospheric variability (Ichoku et al., 2003; Remer et al., 2005). With the accumulation of global AERONET observations, generalized dynamic aerosol models have been developed to further improve MODIS aerosol products. Currently, aerosol information is available from two major MODIS aerosol retrieval algorithms: the MODIS Level-2 aerosol optical depth product (MOD04/MYD04) (Levy et al., 2007a; Levy et al., 2007b) and the MODIS atmospherically corrected surface reflectance product (MOD09/MYD09) (Dubovik et a;., 2002; Lyapustin et al., 2021; Vermote et al., 2006b; Vermote et al., 2008), which employ distinct dynamic aerosol modeling schemes proposed by Levy et al. and Dubovik et al., respectively. These aerosol products have been widely utilized in operational applications, including NASA's Web-enabled Landsat Data (WELD) project for improving Landsat 7

https://doi.org/10.5194/egusphere-2026-1320
Preprint. Discussion started: 7 April 2026

SR data and the atmospheric correction of land observations acquired by the VIIRS sensor onboard the NPP satellite (Roy et al., 2010; Superczynski et al., 2017). Overall, while fixed aerosol models remain widely adopted due to their stability and ease of implementation, dynamic aerosol models provide improved adaptability under complex atmospheric conditions. Compared with fixed aerosol types such as urban, rural, and maritime aerosols, dynamic aerosol models can adjust their optical properties with varying AOD and therefore offer broader applicability across diverse atmospheric environments. However, their performance has not been comprehensively evaluated across different atmospheric correction frameworks. In practice, major aerosol and AC products, such as MOD04, MOD09, and the LaSRC algorithm, employ distinct dynamic aerosol models, yet systematic inter-comparisons among these models remain limited. The use of different aerosol representations may introduce inconsistencies in AOD retrieval (Grey et al., 2006), which can subsequently propagate into SR uncertainties. Therefore, a comparative assessment of widely used dynamic aerosol models is essential for improving retrieval accuracy and optimizing aerosol model selection (Zhang et al., 2022).

Among dynamic aerosol-related products, the Landsat 8 SR product generated by the LaSRC algorithm is one of the most widely used surface reflectance datasets. The performance of Landsat 8 SR products under specific surface and atmospheric conditions still requires further investigation. Previous validation studies have reported systematic deviations over high-reflectance surfaces such as desert playas, where SR tends to be underestimated, particularly in short-wavelength visible bands including coastal aerosol and blue bands (Mann et al., 2024; Meghraj et al., 2023). In addition, product documentation and independent validation studies indicate that uncertainties in SR retrieval increase under challenging atmospheric or illumination conditions, with larger errors frequently observed in shorter visible wavelengths (Roy et al., 2014; Vermote et al., 2016). Existing SR validation efforts are also restricted by limited site coverage and narrow reflectance ranges. For instance, Vermote et al. (Vermote et al., 2006b) validated the LaSRC algorithm using only 33 sites, with SR evaluation in visible bands primarily confined to low-reflectance conditions. These limitations highlight the necessity of systematic validation across diverse aerosol models, surface types, and reflectance ranges. Future research should therefore focus on improving SR retrieval accuracy over high-reflectance surfaces and establishing robust AOD validation frameworks to enhance the reliability of dynamic aerosol modeling in AC applications.

This study presents a comprehensive evaluation of the impacts of widely used dynamic aerosol models on Landsat 8 atmospheric correction performance using multisite observations, long-term temporal datasets, and full reflectance range assessment. Three representative dynamic aerosol models derived from MOD04, MOD09, and the LaSRC Urban Clean aerosol scheme are investigated. Their performance is evaluated through comparative analysis of AOD and SR retrieval accuracy under diverse environmental conditions. The results aim to provide guidance for optimizing aerosol model selection and improving AC performance in operational remote sensing applications.

https://doi.org/10.5194/egusphere-2026-1320
Preprint. Discussion started: 7 April 2026

2 Data sources and characteristics

2.1 Landsat 8 dataset

Landsat 8 satellite data were selected as the primary data source to satisfy the stability and temporal continuity requirements of quantitative analysis. As in several previous studies, 100 globally distributed AERONET sites (Holben et al.,1998) were systematically selected to produce a validation-referenced SR series spanning the entire year 2022. The geographical distributions of these sites are shown in Fig. 1, overlaid on global climate zones. The number of sites by continent is summarized in Table 1, illustrating the global coverage of the dataset. In addition, the sites span 12 major climate zones, with the largest numbers located in humid cold temperate (Df, 26 sites) and humid warm temperate (Cf, 26 sites) regions, followed by warm summer-dry (Cs, 10 sites), tropical savanna (Aw, 7 sites), steppe (Bs, 8 sites), desert (Bw, 8 sites), warm winter-dry (Cw, 5 sites), subarctic continental (Ds, 4 sites), tropical rainforest (Af, 4 sites), subarctic monsoon (Dw, 1 site), and ice-cap (ET, 1 site) climates. This distribution demonstrates that the selected sites provide broad spatial and climatic representativeness, which is essential for evaluating the robustness of AC methods across diverse environmental conditions.

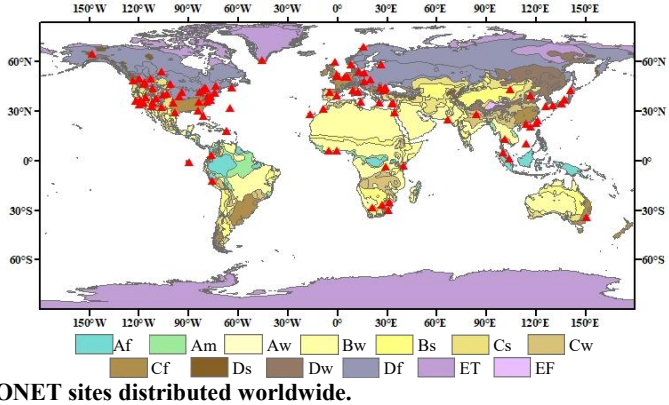

Figure 1: The selected 100 AERONET sites distributed worldwide.

Table 1. Number of AERONET sites used by continent (N = 100).

Continent	Number of Sites
Africa	9
Asia	20
Europe	24
Oceania	1
North America	43
South America	3

Launched on February 11, 2013, as the eighth satellite in the US Landsat program, Landsat 8 carries two key sensors: an Operational Land Imager (OLI) and a Thermal Infrared Sensor (TIRS). Landsat 8 has 11 spectral bands, including nine

https://doi.org/10.5194/egusphere-2026-1320
Preprint. Discussion started: 7 April 2026

multispectral OLI bands covering the VIS to shortwave infrared (SWIR) spectrum (433-2300 nm) and two TIRS thermal infrared bands (10.6-12.51 μm) designed for land surface temperature and moisture monitoring through terrestrial thermal radiation measurements (Roy et al., 2014).

This study utilized the first seven bands of both Landsat 8 Tier 1 Level 1 and Level 2 products with high-quality radiometric correction and orthorectification (Dwyer et al., 2018). Detailed band information is provided in Table 2. In total, more than 3,800 Landsat 8 scenes were identified at the selected 100 AERONET sites for the year 2022. However, 634 scenes were retained as the final dataset (Fig. 2) after rigorous spatiotemporal matching (e.g., image selection based on site coordinates) and quality screening (e.g., excluding images with cloud cover of >20% through QA bands). To ensure spatial homogeneity and reliability, all scenes were processed using the Google Earth Engine (GEE) platform, with each image cropped to a 6 × 6 km square centered on each AERONET site—a finer window than the 9 × 9 km size commonly used in previous validation studies (Doxani et al., 2023).

Table 2. Landsat 8 bands in the reflected solar spectraum.

	Band Range (μ m)	SNIR	SR (m)
Band1-COASTAL/AEROSOL	0.43-0.45	130	30
Band2-Blue	0.45-0.51	130	30
Band3-Green	0.53-0.59	100	30
Band4-Red	0.64-0.67	90	30
Band5-NIR	0.85-0.88	90	30
Band6-SWIR1	1.57-1.65	100	30
Band7-SWIR2	2.11-2.29	100	30

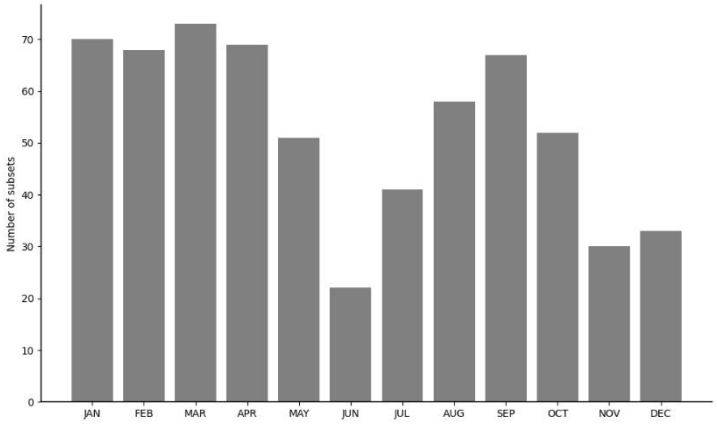

Figure 2: Monthly distribution of the 6 × 6 km Landsat 8 subsets across 100 AERONET sites (Fig. 1) for the year 2022.

https://doi.org/10.5194/egusphere-2026-1320
Preprint. Discussion started: 7 April 2026

Such a standardized processing strategy is required for the validation of atmospheric parameters (e.g., AOD) and SR retrieval to ensure the representation of AERONET measurements over a reasonable spatial extent.

2.2 AOD reference dataset

AERONET (Holben et al.,1998) is a fundamental ground-based observation network in atmospheric sciences that provides globally distributed, high-precision, and high-temporal-resolution aerosol optical parameters. It provides AODs in multiple spectral bands of automated sun photometers, enabling the interpolation of AOD at 550 nm (AOD_{550}), a wavelength commonly used as a key indicator to assess the aerosol concentration and distribution in the atmosphere.

Level-2 AOD data for 2022 were used because of their high quality, ensuring higher precision (with an uncertainty of 0.01–0.02) and stability with cloud screening and instrument calibration (Giles et al., 2019), making them well-suited for AOD comparison studies. To ensure temporal consistency between Landsat 8 imagery and AERONET observations and broader validation coverage across diverse regions, AOD retrievals were selected within $\pm$15 min of Landsat 8 overpass time. The AOD_{550} was then interpolated using measurements at two adjacent wavelengths (440 and 675 nm) by assuming the Junge distribution, as shown in Eq. (1–3):

$$\tau(0.55) = \beta * 0.55^{-\alpha}, \quad (1)$$

$$\alpha = -\frac{\ln \frac{\tau(\lambda_1)}{\tau(\lambda_2)}}{\ln \frac{\lambda_1}{\lambda_2}}, \quad (2)$$

$$\beta = \frac{\tau(\lambda_1)}{\lambda_1^{-\alpha}} = \frac{\tau(\lambda_2)}{\lambda_2^{-\alpha}}. \quad (3)$$

where, $\tau(\lambda_1)$, $\tau(\lambda_2)$ represents the AOD at 440 nm and 675 nm, while α and β denote the Ångström exponent (Ångström, 1964) and the turbidity coefficient, respectively.

2.3 Surface reflectance reference dataset

Common sources of reference data for satellite SR retrieval validation include in-situ ground spectral measurements, other SR products with high accuracy, and AERONET-based SR associated with an accurately validated radiative transfer code. While the first source seems to be direct validation data, it lacks systematic measurements with adequate spatial and spectral resolutions. Instead, indirect validation using the latter two reference sources has been used extensively for SR product comparison (Vermote et al., 2016). In practice, MODIS SR is used as a reference dataset owing to its well-established reliability. However, the spectral and spatial differences between MODIS and Landsat 8 introduce additional errors. Therefore, the AERONET-based SR using the vector 6S 4.1 (Vermote et al., 1997) code (hereafter referred to as 6SV),

https://doi.org/10.5194/egusphere-2026-1320
Preprint. Discussion started: 7 April 2026

accounting for the polarization effect with a mean relative accuracy of 0.4–0.6% (Vermote et al., 2006a), was adopted as the 'true' to validate other Landsat SR retrieved by different approaches.

The critical input parameters for 6SV to compute the SR of Landsat 8 scenes included: 1) spectral response functions (SRF) of Landsat 8 OLI; 2) elevations for AERONET sites; 3) atmospheric models (e.g., mid-latitude summer/winter) estimated based on data acquisition dates and site locations; 4) aerosol properties, including aerosol particle size distribution from AERONET Level 2.0 inversion products, and AOD550 interpolated from AERONET spectral AOD retrievals; 5) geometric imaging parameters, including solar zenith, solar azimuth, viewing zenith, and viewing azimuth; and 6) image acquisition date and time.

3 Methodology

3.1 Atmospheric correction method

This section delineates the AC methodology, focusing on five key aspects: radiative transfer principles, look-up table (LUT) construction, aerosol-type selection, AOD retrieval, and other auxiliary parameter acquisition. To comprehensively evaluate the advantages and limitations of different aerosol types on AC, three dynamic aerosol types (MOD04-based, MOD09-based, and Urban Clean) were used for Landsat 8 AC to retrieve AOD and SR.

1) **Atmospheric correction principle**

The solar radiation received by the sensor consists of both surface-reflected and atmospheric-scattered components. Assuming a Lambertian surface and considering atmospheric absorption and scattering, these contributions can be reformulated in terms of the top-of-atmosphere (TOA) reflectance. For narrow spectral bands outside the major water vapor absorption features, TOA reflectance can be calculated as follows (Vermote et al., 2008):

$$\rho^*(\theta_s,\theta_v,\varphi,P,Aer,U_{H_2O},U_{O_3}) = T_{g_{OG}}(m,P)T_{g_{O_3}}(m,U_{O_3})\cdot[\rho_{atm}(\theta_s,\theta_v,\varphi,P,Aer,U_{H_2O}) + Tr_{atm}(\theta_s,\theta_v,P,Aer)\frac{\rho_t}{1-S_{atm}(P,Aer)\cdot\rho_t}T_{g_{H_2O}}(m,U_{H_2O})], \quad (4)$$

where $\rho^*(\theta_s,\theta_v,\varphi,P,Aer,U_{H_2O},U_{O_3})$ represents the TOA reflectance, θ_s represents the solar zenith angle, θ_v represents the view zenith angle, and φ represents the relative azimuth angle. P is the atmospheric pressure, and Aer describes aerosol properties, including AOD, aerosol single-scattering albedo, and phase function. where U_{H_2O} and U_{O_3} represent the water vapor content (WVC) and ozone content, respectively. Additionally, $T_{g_{H_2O}}$, $T_{g_{O_3}}$, and $T_{g_{OG}}$ are the gaseous transmissions of water vapor, ozone, and other gases, respectively; where $\rho_{atm}(\theta_s,\theta_v,\varphi,P,Aer,U_{H_2O})$ denotes the atmospheric intrinsic reflectance, $Tr_{atm}(\theta_s,\theta_v,P,Aer)$ represents the total atmospheric transmittance, and ρ_t represents the SR retrieved by the AC procedure, and $S_{atm}(P,Aer)$ represents the atmospheric spherical albedo.

To simplify the computational processes in Eq. (4), we employ the approach used by Vermote et al. for MODIS (Vermote et al., 2006b). This method separately addresses the atmospheric absorption and scattering effects, thereby considerably reducing the complexity and storage requirements for LUT construction. The first step involved correcting the TOA

https://doi.org/10.5194/egusphere-2026-1320
Preprint. Discussion started: 7 April 2026

reflectance (hereafter referred to as the corrected TOA reflectance) for absorption effects, including adjustments for general gas absorption (excluding water vapor and ozone), ozone absorption, and water vapor. The corrected TOA reflectance can be expressed as follows:

$$\rho_c^*(i) = \frac{1}{T_{g_{OG}}^i(m,P)\cdot T_{g_{O_3}}^i(m,U_{O_3})\cdot T_{g_{H_2O}}^i(m,U_{H_2O})}\rho^*(i) \quad , \tag{5}$$

$$T_{g_{OG}}^i(m,P) = \exp[m(a_0^i P + a_1^i \ln(P)) + \ln(m)(b_0^i P + b_1^i \ln(P)) + m\ln(m)(c_0^i P + c_1^i \ln(P))] \, , \tag{6}$$

$$T_{g_{O_3}}^i(m,U_{O_3}) = \exp(-m a_{O_3}^i U_{O_3}) \quad , \tag{7}$$

$$T_{g_{H_2O}}^i(m,U_{H_2O}) = \exp[a_{H_2O}^i m U_{H_2O} + b_{H_2O}^i \ln(mU_{H_2O}) + c_{H_2O}^i mU_{H_2O}\ln(mU_{H_2O})], \tag{8}$$

$$m = \frac{1}{\cos(\theta_s)} + \frac{1}{\cos(\theta_v)} \quad , \tag{9}$$

where i is the Landsat 8 band number, m is the relative atmospheric air mass, and P is atmospheric pressure (atm). The parameters a_0^i, a_1^i, b_0^i, b_1^i, c_0^i, c_1^i, $a_{O_3}^i$, $a_{H_2O}^i$, $b_{H_2O}^i$, and $c_{H_2O}^i$ are associated with the SRFs of Landsat 8. The parameters for the different Landsat 8 bands were retrieved by running the 6SV code under different atmospheric conditions. The corrected TOA reflectance is expressed as follows:

$$\rho_c^*(\theta_s,\theta_v,\varphi,P,Aer,U_{H_2O},U_{O_3}) = \frac{\rho_{atm}(\theta_s,\theta_v,\varphi,P,Aer,U_{H_2O})}{T_{g_{H_2O}}(m,U_{H_2O})} + Tr_{atm}(\theta_s,\theta_v,P,Aer)\frac{\rho_t}{1-S_{atm}(P,Aer)\cdot\rho_t} \quad , \tag{10}$$

A further approximation allows unknown atmospheric parameters (ρ_{atm}, Tr_{atm}, S_{atm}) to be computed only at standard pressure , leading to an additional reduction in lookup table size. The relevant formulas are as follows:

$$\rho_{atm}(\theta_s,\theta_v,\varphi,P,Aer,U_{H_2O}) = \rho_R(\theta_s,\theta_v,\varphi,P) + \left[\rho_{R+Aer}(\theta_s,\theta_v,\varphi,P_0,Aer) - \rho_R(\theta_s,\theta_v,\varphi,P_0)\right]\cdot T_{g_{H_2O}}(m,\frac{U_{H_2O}}{2}) \, , \tag{11}$$

$$\rho_R(\theta_s,\theta_v,\varphi,\tau_R(P)) = \rho_R(\theta_s,\theta_v,\varphi,\tau_R\cdot P/P_0) \, , \tag{12}$$

$$Tr_{atm}(\theta_s,\theta_v,P,Aer) = T_{atm}(\theta_s,P,Aer)T_{atm}(\theta_v,P,Aer) \, , \tag{13}$$

$$T_{atm}(\theta,P,Aer) = T_{atm}(\theta,P_0,Aer)\frac{T_R(\theta,P)}{T_R(\theta,P_0)} \quad , \tag{14}$$

$$S_{atm}(P,Aer) = \left(S_{atm}(P_0,Aer) - S_R(P_0)\right) + S_R(P) \, , \tag{15}$$

$$S_R(P) = \frac{1}{4+3P/P_0\cdot\tau_R}\left[3P/P_0\cdot\tau_R - 4E_3(P/P_0\cdot\tau_R) + 6E_4(P/P_0\cdot\tau_R)\right] \, . \tag{16}$$

where ρ_{R+Aer} represents the aerosol and Rayleigh scattering effects, and τ_R is the Rayleigh optical thickness. T_R represents the atmosphere transmission function due to molecular scattering, T_{atm} is the upwelling or downwelling atmospheric

https://doi.org/10.5194/egusphere-2026-1320
Preprint. Discussion started: 7 April 2026

transmittance, and S_R is the Rayleigh spherical albedo. And E_3, E_4 are exponential integral function.

Through the two-step simplification, the AC process ultimately requires only a limited set of unknown atmospheric parameters, including τ_R, ρ_{R+Aer}, T_{atm}, S_{atm} at standard atmospheric pressure, AOD, WVC, ozone content, and atmospheric pressure P. The following section provides a detailed description of the unknown parameters.

2) **LUT construction**

In the remote sensing domain of AC and atmospheric parameter retrieval, RTMs account for multiple complex atmospheric radiation processes that require large amounts of computation. However, it is impossible to run RTMs directly for large-scale image processing owing to their high time costs. Therefore, the LUT technique is typically used for this purpose. LUTs precompute and store RTM-based results under various conditions, enabling rapid retrieval of atmospheric parameters through interpolation between discrete nodes. This approach substantially reduces redundant computations and enhances the processing efficiency. LUT-based methods are widely used in remote sensing, and numerous AC software packages, such as ISDAS (Staenz et al., 1997; Staenz et al., 1998), ATCOR (Schläpfer et al., 2002; Brazile et al., 2008; Perkins et al., 2012a; Perkins et al., 2012b), Atmospheric Removal Program (ATREM) (Gao et al., 1992), MODIS product processing system (Toller et al., 2009), and LEDAPS (Masek et al., 2006), utilize RTMs (e.g., MODTRAN or 6S) to pre-construct LUTs to accelerate the processing procedures.

In this study, a dynamic aerosol-type LUT was constructed using the 6SV code to enable the efficient interpolation of AC parameters under varying aerosol conditions, offering greater adaptability compared to conventional fixed-type LUTs. To accommodate the diverse atmospheric and geometric configurations encountered in real-world scenes, the LUT includes six input parameter dimensions (Table 3): viewing zenith angle (VZ), solar zenith angle (SZ), relative azimuth angle (RAA), aerosol type (AerT), 550 nm AOD (AOD550), and spectral band (Band). For each parameter combination, the LUT outputs the corresponding atmospheric radiative parameters, assuming a standard atmospheric pressure. The concentrations of water vapor and ozone were fixed at 1.0 g·cm^{-2} and 300 cm-atm, respectively, as their spatial and temporal variations exert only minor influences on the TOA. Accounting for these variables would considerably increase the computational and storage requirements without substantially improving accuracy (Guanter et al., 2009). Consequently, the six selected parameters were considered sufficient to characterize the atmospheric conditions pertinent to this study.

Table 3. LUT variables settings.

Variables	Setting
VZ	0,12,24,36
SZ	1.5,12,24,36,48,54,60,66,72
RAA	0,30,60,90,120,150,180
Aerosol Type (AerT)	MOD04-based: Strongly Absorbing, Moderately Absorbing, Weakly Absorbing, Spheroid/Dust MOD09-based: Urban Clean, Urban Polluted, Smoke Low Absorption, Smoke High Absorption, Dust
AOD_{550}	0.01,0.05,0.1,0.15,0.2,0.3,0.4,0.6,0.8,1,1.2,1.4,1.6,1.8,2,2.3,2.6,3,3.5,4,4.5,5.0

https://doi.org/10.5194/egusphere-2026-1320
Preprint. Discussion started: 7 April 2026

Band	1、2、3、4、5、6、7

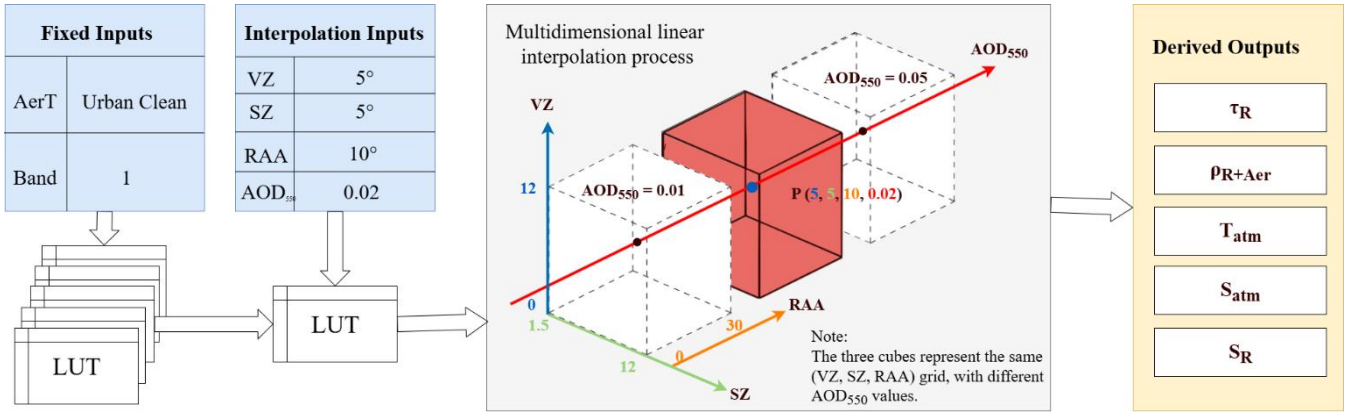

Figure 3: Input–Output Framework for Atmospheric Radiative Transfer Calculations Using Multidimensional LUT.

In total, 349,272 valid parameter combinations were generated for the six variables. Each combination was systematically computed using 6SV code, compiled into an LUT, and converted into a binary format to reduce the storage footprint. Fig. 3 demonstrates the multidimensional linear interpolation process for retrieving AC parameters when AerT = Urban Clean, Band = 1, VZ = 5°, SZ = 5°, RAA = 10°, and AOD_{550} = 0.02. First, the appropriate sub-LUT is selected according to the specified aerosol type (AerT) and spectral band (Band). Then, for a given observation geometry (VZ, SZ, RAA) and aerosol AOD (AOD_{550}), the required parameters are obtained through multidimensional linear interpolation among the nearest neighboring nodes in the LUT. The interpolated results provide the AC parameters (τ_R , ρ_{R+Aer} , T_{atm} , S_{atm} , S_R) required for SR retrieval.

3) **Dynamic aerosol type selection**

This study incorporated three representative dynamic aerosol types: MOD04-based, MOD09-based, and Urban Clean, all of which were derived from global AERONET results. Specifically, aerosol-subtype selection for MOD04-based adheres to seasonal and regional characteristics, whereas MOD09-based aerosol subtypes are optimized using error minimization criteria. Urban Clean, operating as an aerosol subtype under MOD09-based conditions, remained aerosol subtype under MOD09-based conditions, remained fixed during the AC in terms of type selection. All three types were parameterized using a bi-lognormal distribution model, with their coefficients dynamically adjusted in response to AOD variations.

a) MOD04-based types

MOD04-based aerosol types employ a fixed classification scheme based on 1°×1° global grid cells, with variations governed by seasonal and regional aerosol distribution patterns. This aerosol-subtype distribution was statistically derived from multiyear AERONET observational datasets, encompassing three fine-mode-dominant subtypes (strongly, moderately, and weakly absorbing) and one coarse-mode-dominant subtype (spheroid/dust). The optical parameters for the four subtypes

https://doi.org/10.5194/egusphere-2026-1320
Preprint. Discussion started: 7 April 2026

were adopted from Levy et al. (Levy et al., 2007). As illustrated in Fig. 4, the quarterly spatial distributions of the three fine-mode and one coarse-mode aerosol subtype were adapted from the methodologies of Levy (Levy et al., 2003) and Friedl (Friedl et al., 2002).

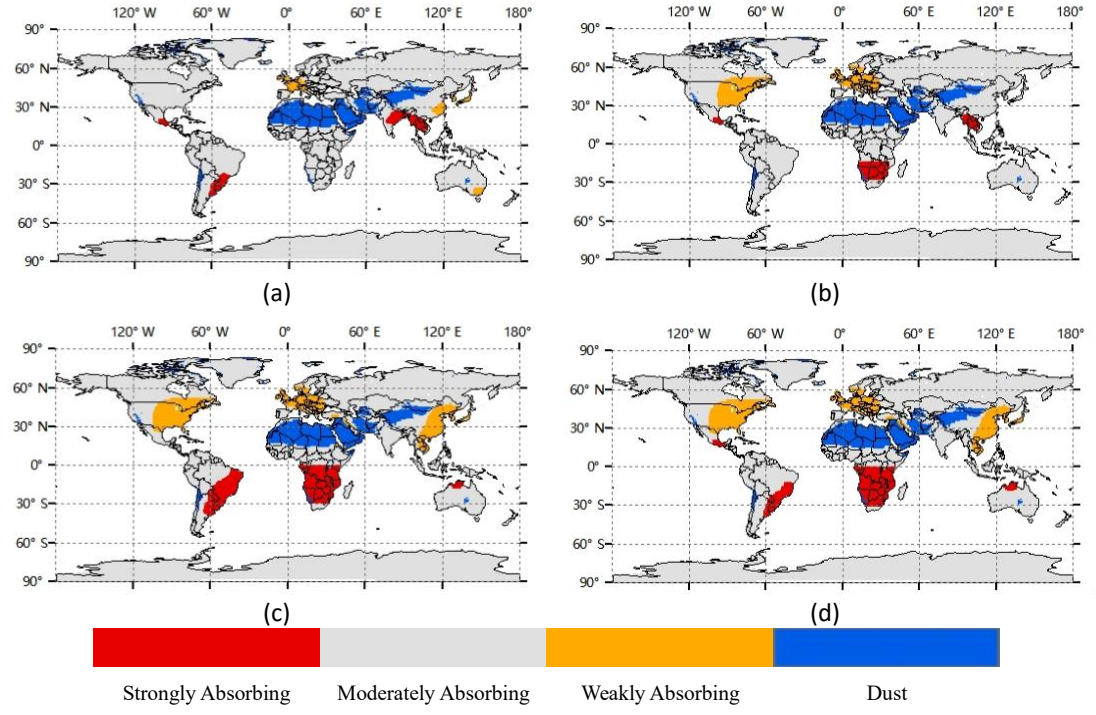

Figure 4: 1°*1°Global land surface aerosol types across different seasons. (a) December, January and February (DJF); (b) March, April and May (MAM); (c)June, July and August (JJA); (d) September, October and November (SON).

b) MOD09-based types

MOD09-based type was statistically derived from eight years of AERONET observational datasets and comprised four subtypes: urban clean, urban polluted, smoke low-absorption, and smoke high-absorption (Remer et al., 2005). Each type was parameterized dynamically using AOD-dependent coefficients. During operational implementation, an additional dust aerosol type (Remer et al., 1998) was incorporated to improve the environmental representativeness and accuracy of AC. For AOD retrieval for a given pixel, the goodness-of-fit residuals for all five candidate subtypes were computed and compared. Subsequently, the type exhibiting the minimum residual is selected for inversion to ensure optimal retrieval accuracy via adaptive model selection.

$$AOD_{MOD09-based} = \arg\min\left(\Delta_{UrbanClean}, \Delta_{UrbanPolluted}, \Delta_{SmokeLow}, \Delta_{SmokeHigh}, \Delta_{Dust}\right), \quad (17)$$

c) Urban Clean

The Urban Clean aerosol type, designated in the official Landsat 8 official AC algorithm (LaSRC), has optical parameters that are dynamically adjusted according to AOD variations (Remer et al., 2005).

https://doi.org/10.5194/egusphere-2026-1320
Preprint. Discussion started: 7 April 2026

4) **AOD retrieval**

The AOD retrieval framework employs MODIS-derived band ratio relationships and Landsat 8-9 ratio files (Vermote et al., 2016) for computational optimization. First, the ratio file generates spectral indices between the deep blue (DB), blue (B), SWIR, and red (R) bands. The $NDVI_{SWIR}$ index substitutes the red band in the Normalized Difference Vegetation Index (NDVI) formula with the SWIR band, maintaining numerical proximity while reducing the sensitivity to aerosols. This parameterization of the ratio as a function of $NDVI_{SWIR}$ enabled the capture of its potential seasonal and interannual variability.

Subsequently, iterative optimization was performed, where residuals were calculated based on band ratio relationships. The AOD value corresponding to the minimum residual was identified through cyclic computation, and subsequently refined using quadratic fitting.

$$Ratio = a * NDVI_{SWIR} + b \quad (18)$$

$$NDVI_{SWIR} = \frac{\rho_t(b_5) - \rho_t(b_7)/2}{\rho_t(b_5) + \rho_t(b_7)/2} \quad (19)$$

$$\Delta = \sqrt{\left(\rho_t(b_1) - Ratio1 \cdot \rho_t(b_4)\right)^2 + \left(\rho_t(b_2) - Ratio2 \cdot \rho_t(b_4)\right)^2 + \left(\rho_t(b_7) - Ratio7 \cdot \rho_t(b_4)\right)^2} \quad (20)$$

where a and b denote the band ratio values, and $\rho_t(b_1)$, $\rho_t(b_2)$, $\rho_t(b_4)$, $\rho_t(b_5)$, and $\rho_t(b_7)$ represent the SR in the deep blue, blue, red, near-infrared, and shortwave infrared bands, respectively.

5) **Auxiliary parameter acquisition**

Atmospheric Pressure: In AC processes, parameters such as path radiance and total atmospheric transmittance are inherently influenced by atmospheric pressure. Consequently, accurate SR retrieval requires a reliable pressure data source. In this study, the atmospheric pressure was estimated based on an empirical relationship with elevation derived from a Digital Elevation Model (DEM). In particular, for each DEM pixel with elevation H (km), the corresponding atmospheric pressure P (atm) was calculated as

$$P = 1013 \cdot \exp(-H/8) \quad (21)$$

Water Vapor Content (WVC): The WVC used in this study was obtained from the National Centers for Environmental Prediction (NCEP) and the National Center for Atmospheric Research (NCAR) Reanalysis dataset developed by the NCEP/NCAR. This global reanalysis product, available since 1948, provides the WVC (kg/m³) with a temporal resolution of 6 h and a spatial resolution of 2.5° × 2.5°. The data were spatially interpolated to image site locations and temporally aligned with the corresponding acquisition time.

Ozone: Ozone data were derived from the Ozone Monitoring Instrument (OMI) onboard NASA's Aura satellite, which is part of the Earth Observing System (EOS). OMI provides daily global ozone column densities in Dobson Units (DU) at a resolution of 2.5° × 2.5°. For each scene, site-specific ozone concentrations were extracted based on geographic location and

https://doi.org/10.5194/egusphere-2026-1320
Preprint. Discussion started: 7 April 2026

image acquisition time.

The integration of these datasets enabled the accurate estimation of atmospheric pressure, WVC, and ozone, which are the three essential inputs for the AC process, thereby enhancing the accuracy of AOD and SR retrievals.

3.2 Accuracy validation method

The accuracy of AOD retrieval was assessed using scatter plots, where the slope and correlation coefficient from the linear regression characterized the agreement between the retrieved and ground truth values. In addition, the root mean square error (RMSE), coefficient of determination (R^2) and Bias were computed to quantify retrieval performance across different aerosol types. These statistical metrics provide an objective basis for evaluating the algorithm performance. The corresponding formulas are as follows:

$$Bias = \frac{1}{n}\sum_{i=1}^{n}\left(AOD_{model} - AOD_{ground}\right), \tag{22}$$

$$RMSE = \sqrt{\frac{1}{n}\sum_{i=1}^{n}\left(AOD_{model} - AOD_{ground}\right)^2}, \tag{23}$$

$$R^2 = 1 - \frac{\sum_{i=1}^{n}\left(AOD_{model} - AOD_{ground}\right)^2}{\sum_{i=1}^{n}\left(AOD_{ground} - \overline{AOD_{ground}}\right)^2}, \tag{24}$$

where AOD_{model}, AOD_{ground} denotes the model-retrieved and ground-truth AOD values, and n represents the total number of image samples. We computed 95% confidence intervals (CIs) for all parameters via bootstrapping (1,000 iterations). Additionally, R^2 values were calculated for both the linear regression fit (R^2_linear) and aerosol-type-specific predictions (R^2_AerT).

Pairwise statistical significance of RMSE and Bias differences between aerosol types was assessed using paired permutation tests, with Holm-adjusted p-values to control the family-wise error rate. R^2_AerT differences were evaluated using Paired bootstrap resampling of ΔR^2_AerT, followed by Holm adjustment. Statistical significance was determined at $\alpha = 0.05$, and results are reported with significance stars (*** $p < 0.001$, ** $p < 0.01$, * $p < 0.05$, ns: not significant).

2) **Surface Reflectance accuracy validation**

To validate the SR, we employed a three-tiered evaluation framework encompassing the overall, per-band, and reflectance-range levels. The assessment is based on three key metrics: accuracy (A), precision (P), and uncertainty (U). These indicators enable a comprehensive evaluation of reflectance performance under varying aerosol types, identifying the errors and uncertainties introduced by each. Specifically, A reflects the agreement between the retrieved and reference values, P indicates result consistency, and U captures the potential error range during the measurement process. The relevant formulas

https://doi.org/10.5194/egusphere-2026-1320
Preprint. Discussion started: 7 April 2026

are as follows (Vermote et al., 2016).

$$A = \frac{1}{n}\sum_{i=1}^{n}\left(\rho_i^e - \rho_i^t\right), \quad (25)$$

$$P = \sqrt{\frac{1}{n-1}\times\sum_{i=1}^{n}\left(\varepsilon_i - A\right)^2}, \quad (26)$$

$$U = \sqrt{\frac{1}{n}\times\sum_{i=1}^{n}\varepsilon_i^{\,2}}, \quad (27)$$

All metrics were accompanied by 95% CIs constructed via bootstrapping (n=1,000).

In addition to the comprehensive accuracy validation described above, we conducted a targeted analysis focusing on five representative land-cover types (building, snow, soil, vegetation, water). For each land-cover category, the corresponding pixels were extracted using commonly-used remote sensing ecological index (RSEI), including the Normalized Difference Building Index (NDBI), the Normalized Difference Snow Index (NDSI), the Bare Soil Index (BSI), NDVI and the Normalized Difference Water Index (NDWI). The corresponding formulas are as follows:

Building: $$NDBI = \frac{\rho_t(b_6) - \rho_t(b_5)}{\rho_t(b_6) + \rho_t(b_5)} > 0, \quad (28)$$

Snow: $$NDSI = \frac{\rho_t(b_3) - \rho_t(b_6)}{\rho_t(b_3) + \rho_t(b_6)} > 0.3, \quad (29)$$

Soil: $$BSI = \frac{\left(\rho_t(b_6) + \rho_t(b_4)\right) - \left(\rho_t(b_5) + \rho_t(b_1)\right)}{\left(\rho_t(b_6) + \rho_t(b_4)\right) + \left(\rho_t(b_5) + \rho_t(b_1)\right)} > 0, \quad (30)$$

Vegetation: $$NDVI = \frac{\rho_t(b_5) - \rho_t(b_4)}{\rho_t(b_5) + \rho_t(b_4)} > 0.1, \quad (31)$$

Water: $$NDWI = \frac{\rho_t(b_3) - \rho_t(b_5)}{\rho_t(b_3) + \rho_t(b_5)} > 0.4. \quad (32)$$

where $\rho_t(b_3)$ and $\rho_t(b_6)$ represent the SR in the green and SWIR bands.

For each land-cover type, the SR retrieval performance across seven spectral bands was quantitatively evaluated using reference data. Statistical performance metrics, including RMSE, Bias, and R^2, were calculated to compare the accuracy of different SR products.

https://doi.org/10.5194/egusphere-2026-1320
Preprint. Discussion started: 7 April 2026

4 Results

4.1 AOD validation results

The scatter plot in Fig. 5, generated from 451 cloud-free images, illustrates the AOD retrieval performance at 550 nm for the MOD04-based, MOD09-based, and Urban Clean dynamic aerosol types. As no official Landsat 8 AOD products are currently available (She et al., 2022), the comparison is limited to these three aerosol types. The x-axis denotes the AERONET observations, and the y-axis shows the corresponding estimated AOD values. The black dashed line denotes the 1:1 reference, which serves as a benchmark for ideal agreement between the retrieved and ground-truth values. Flanking this line, the black solid lines delineate the empirical uncertainty envelope—defined as $0.15 \times AOD_{550} \pm 0.05$—based on the empirical uncertainty of MODIS land AOD retrievals (Remer et al., 2005). The solid blue line represents the least-squares regression fit, which highlights the relationship between the two datasets. To assess AOD retrieval accuracy, three statistical metrics, RMSE, bias, and coefficient of determination (R2_AerT), were calculated (Table 4).

The results indicated noticeable differences among the scatter plots for the three dynamic aerosol types. In terms of scatter distribution, most MOD0-based data points fell within the uncertainty range (blue solid lines) and were relatively concentrated. The Urban Clean type followed, displaying a relatively uniform distribution, but appearing slightly more dispersed than the MOD04-based type. In contrast, MOD09-based type exhibited the highest dispersion, with a significant proportion of points falling outside the uncertainty bounds, indicating a greater variability in the data.

Upon further examination of the regression lines, the slopes for the MOD04-based, MOD09-based, and Urban Clean types were 0.9047, 1.0852, and 1.0295, respectively. The Urban Clean regression line was the closest to the 1:1 reference line, suggesting an optimal fit. The MOD04-based regression line, with a slope of less than one, intersects the 1:1 line, indicating a degree of bias. By contrast, the MOD09-based regression line exhibited the greatest deviation from the 1:1 line, suggesting a less accurate fit.

According to the accuracy metrics in Table 4, the RMSE values ranged from 0.0437 to 0.0612, Bias values ranged from 0.0052 to 0.0264, and R^2_AerT values ranged from 0.4586 to 0.7236. Statistical significance was assessed using paired permutation tests for RMSE and Bias, and paired bootstrap resampling for ΔR^2_AerT, followed by Holm correction for multiple comparisons. The results in Table 5 indicate that RMSE and Bias differences between all model pairs were statistically significant ($p < 0.001$, ***), with MOD04-based significantly outperforming MOD09-based and Urban Clean, and Urban Clean outperforming MOD09-based. In contrast, although R^2_AerT differences showed consistent trends (MOD04-based > Urban Clean > MOD09-based), the bootstrap confidence intervals for ΔR^2_AerT overlapped zero in several comparisons, and none of the R^2_AerT differences reached statistical significance after multiple-comparison adjustment. These findings demonstrate that MOD04-based consistently provides the most accurate and least biased AOD estimates, while improvements in goodness-of-fit over other types are less robust statistically.

Overall, although the three aerosol types yielded comparable results, differences remained in their specific RMSE, bias, and R^2 values. The MOD04-based type demonstrated the best performance across all three metrics, indicating higher accuracy,

https://doi.org/10.5194/egusphere-2026-1320
Preprint. Discussion started: 7 April 2026

followed by Urban Clean, whereas the MOD09-based type exhibited the weakest performance across all indicators.

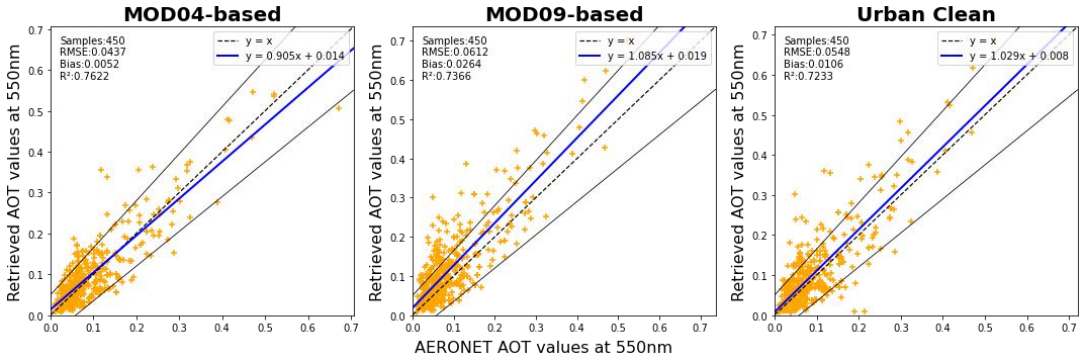

Figure 5: Dispersion plot of 550 nm aerosol optical thickness(specs=0.15×AOD550+0.05).

Table 4. Accuracy metrics for aerosol optical thickness.

	MOD04-based	MOD09-based	Urban Clean
RMSE	0.0437[0.0392, 0.0486]	0.0612 [0.0556, 0.0668]	0.0548 [0.0488, 0.0606]
R^2_AerT	0.7236 [0.6161, 0.8077]	0.4586 [0.2617, 0.6157]	0.5653 [0.3889, 0.6993]
Bias	0.0052 [0.0014, 0.0090]	0.0264 [0.0214, 0.0316]	0.0106 [0.0059, 0.0155]

Table 5. Statistical significance of differences in performance metrics among aerosol types (HOLM correction applied).

Comparison	Metric	Mean Diff	Holm-adjusted p	Significance
MOD04-based vs MOD09-based	Bias	−0.021232	0.00015	***
MOD04-based vs Urban Clean	Bias	−0.005385	0.00075	***
MOD09-based vs Urban Clean	Bias	0.015847	0.00010	***
MOD04-based vs MOD09-based	RMSE	-0.001839	0.00015	***
MOD04-based vs Urban Clean	RMSE	−0.001096	0.00010	***
MOD09-based vs Urban Clean	RMSE	0.000744	0.00030	***
MOD04-based vs MOD09-based	R2_AerT	0.257920	1.00000	ns
MOD04-based vs Urban Clean	R2_AerT	0.153634	1.00000	ns
MOD09-based vs Urban Clean	R2_AerT	−0.104286	0.94600	ns

Note: *** $p < 0.001$, ** $p < 0.01$, * $p < 0.05$, ns = not significant.

4.2 SR validation results

A total of 634 images were systematically analyzed to validate the SR accuracy. To maximize the utilization of all available pixels for validation, per-pixel cloud detection was performed on each image prior to accuracy assessment, and only cloud-free pixels were used for validation. Using predefined metric formulations, we calculated Accuracy-Precision-Uncertainty

https://doi.org/10.5194/egusphere-2026-1320
Preprint. Discussion started: 7 April 2026

(APU) values by comparing the reflectance retrievals derived from the three dynamic aerosol types against the 6SV-simulated ground truth. For comparison, the same validation procedure was applied to the Landsat 8 LaSRC SR product to enable direct assessment of the algorithmic performance. To ensure a comprehensive evaluation, the results were presented across three analytical dimensions: overall, per band, and reflectance range assessments.

1)**Overall assessment**

The overall assessment was conducted by computing the total A, P, and U values of the four SR products. Table 6 presents the results. The total A, P, and U values for the four SR products are 0.00036–0.00377, 0.02382–0.02544, and 0.02337–0.2598, respectively.

Among these products, MOD04-based and Urban Clean exhibited a notably higher A value, indicating that the SR retrieved using these two dynamic aerosol types exhibited a higher systematic error, with a consistent offset across all observations. Regarding random error (P value) and overall accuracy (U value), the differences between the four SR products were minimal, indicating that their random errors and overall accuracies were comparable.

Using 95% confidence intervals, we formally assessed pairwise differences in A, P, and U across the four types. The confidence intervals for the between-model differences excluded zero, showing statistically significant disparities in all metrics. Despite exhibiting a certain degree of bias, The MOD04-based type had the lowest P (0.023184) and U (0.023366) values, meaning the highest precision and lowest uncertainty.

Table 6. Overall A, P and U of four SR products.

	A	P	U
MOD04-based	3.0145 [3.0111, 3.0178]	2.3184 [2.3181, 2.3186]	2.3366 [2.3310, 2.23418]
MOD09-based	0.7451 [0.7416, 0.7486]	2.4274 [2.4272, 2.4277]	2.4304 [2.4258, 2.24355]
Urban Clean	1.1465 [1.1431, 1.1500]	2.3870 [2.3872, 2.3877]	2.3911 [2.3857, 2.23963]
LaSRC	-0.2975 [-0.3013, -0.2937]	2.6020 [2.6017, 2.6022]	2.6040 [2.5966, 2.26112]

2)**Per-band assessment**

To visually assess the A, P, and U values of the SR across the seven bands for the four products, we computed the corresponding accuracy metrics (CI = 95%) and generated a heatmap (Fig. 6). The heatmap uses color intensity to intuitively display value magnitudes, with darker shades representing lower values and greater accuracy.

For A values, heatmap analysis indicated that MOD04-based, MOD09-based, Urban Clean, and LaSRC vary across different spectral bands. Specifically, MOD04-based had the smallest A values in the first and second bands, MOD09-based performed best in the third band, and LaSRC outperformed the others in the fourth to seventh bands. The A-value evaluation results were consistent with the overall assessment phase, indicating that MOD09-based and LaSRC demonstrated lower systematic errors compared to MOD04-based and Urban Clean. The P and U values follow a similar pattern, showing a decreasing trend with increasing wavelength. Specifically, the MOD04-based type demonstrated a higher accuracy in the visible bands (first to fourth bands), Urban Clean performed better in the NIR band (fifth band), whereas LaSRC exhibited

https://doi.org/10.5194/egusphere-2026-1320
Preprint. Discussion started: 7 April 2026

superior performance in the SWIR bands (sixth and seventh bands).

In general, the per-band assessment provided a more detailed extension of the overall results. Notably, the four SR products exhibited substantial differences in systematic error (A value), with each product showing strengths in different spectral bands. In contrast, differences in random error (P value) and overall accuracy (U value) were relatively minor, indicating comparable retrieval performance among the products. MOD04-based showed the largest overall systematic error, with superior performance limited to the deep blue and blue bands. MOD09-based and Urban Clean exhibited similar accuracy across all metrics. LaSRC demonstrated the lowest A, P, and U values in the shortwave bands, suggesting a clear advantage in that spectral region.

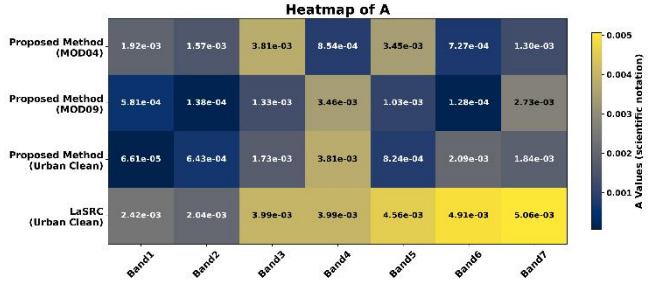

(a) A values of four SR products in single bands

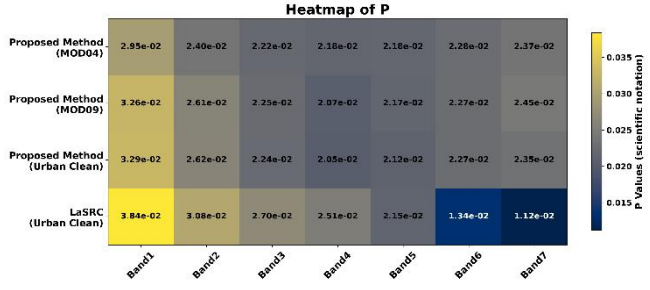

(b) P values of four SR products in single bands

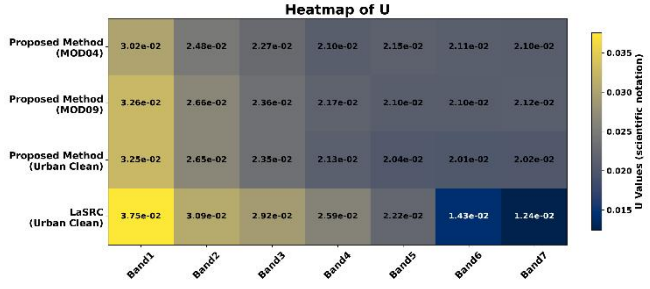

(c) U values of four SR products in single bands

Figure 6: Thermal map of the A, P and U of four SR products in single bands.

3) **Reflectance-range assessment**

To further analyze the accuracy of SR, the 0–1 reflectance range was divided into 0.05 intervals, and accuracy metrics were computed for each interval to validate SR across the full range (CI = 95%). Fig. 7 illustrates the results: the x-axis represents SR values within the 0-1 range, the left y-axis denotes the number of pixels (with tick marks at 10^4, 10^5, 10^6, 10^7, and 10^8),

https://doi.org/10.5194/egusphere-2026-1320
Preprint. Discussion started: 7 April 2026

and the right y-axis presents accuracy metrics. Gray bars denote pixel counts per interval, and the red, green, while red, green, and blue dashed lines represent A, P, and U, respectively. The purple dashed line represents the error line, defined as: S_line = 0.15 × ρ + 0.015.

As shown in Fig. 7, all products exhibited similar pixel distribution patterns. Most pixels were concentrated in the 0–0.3 reflectance range, especially in low-to-medium ranges across all bands. Therefore, subsequent analysis focused on this range to reflect the domin · ant pixel distribution and ensure robust SR performance evaluation.

In this section, we categorize the spectral bands based on the overall and per-band assessments. Using the accuracy validation metrics and error lines shown in Fig. 7, SR performance was analyzed for VIS (bands 1–4), NIR (band 5), and SWIR (bands 6 and 7).

VIS bands: Within the visible spectral bands, the A, P, and U values for all four products exhibited an overall increasing trend with increasing SR, indicating amplified systematic errors, random errors, and total uncertainties as reflectance increased. However, performance variations among the products highlight common trends and distinct characteristics in SR retrieval.

The A values for most algorithms remained below the error thresholds across the 0°–0.45° reflectance range, with relatively flat curves showing a peak interval near 0.25–0.30. During this phase, the deep blue and blue bands exhibit higher A values than the other visible bands. Beyond 0.45, A increased monotonically. LaSRC exhibited the most pronounced upward trend, consistently yielding higher A values than the other algorithms, indicating a greater systematic bias under high-reflectance conditions. MOD09-based and Urban Clean showed similar behavior, with deep blue/blue band A values largely below thresholds, whereas green/red bands displayed significant deviations above thresholds at reflectance >0.8 (except for the MOD09-based in the red band). MOD04-based maintained stability up to 0.8 reflectance but showed a sharp A value spike near 0.85, surpassing MOD09-based and Urban Clean.

The P values in the VIS bands followed smooth trajectories with three distinct peaks. The first two peaks occurred at 0.15–0.20 and 0.25–0.30, predominantly in the deep blue and blue bands. MOD04-based type achieved lower and more stable P values in these ranges, whereas MOD09-based and Urban Clean type exhibited higher peaks, indicating weaker control over random errors. LaSRC exhibited the highest second peak in the deep blue bands, reflecting significant random errors. A third abrupt P-value increase emerges near 0.6 reflectance, with error magnitudes increasing with wavelength. MOD04-based displays minimal increments, exceeding thresholds only in the green/red bands, while MOD09-based and Urban Clean display comparably higher peaks across broader reflectance ranges. The P values of LaSRC persistently exceeded the thresholds above a reflectance of 0.5, indicating severe random errors. Notably, MOD04-based, MOD09-based, and Urban Clean surpassed the error thresholds in the high-reflectance range (>0.8).

Mirroring P value trends, U values peak at 0.15–0.20 reflectance in deep blue/blue bands for MOD04-based, MOD09-based, and Urban Clean, with LaSRC showing negligible peaks. The MOD04-based minimal peaks confirm the superior precision of the low-reflectance regimes. All the algorithms exhibited monotonically increasing U values with reflectance. MOD04-based excelled in the low-to-moderate range, whereas MOD09-based and Urban Clean stabilized at higher reflectance.

https://doi.org/10.5194/egusphere-2026-1320
Preprint. Discussion started: 7 April 2026

LaSRC performed the worst above 0.8 reflectance, with markedly elevated U values.

Overall, in the VIS bands, the MOD04-based type achieved optimal A/P/U performance in the low-to-moderate reflectance range, whereas the MOD09-based type minimized errors at high reflectance. Urban Clean metrics closely aligned with MOD09-based metrics but were marginally higher. The LaSRC product demonstrated the largest errors across the VIS bands and did not exhibit any advantages in these spectral ranges.

NIR bands: In the NIR band, all four products exhibited an overall increasing trend in A, P, and U values with increasing SR.

The MOD04-based, MOD09-based, and Urban Clean-based A values exhibited peak values in the high SR range. MOD04-based peaks at reflectance values between 0.90 and 0.95, with A values in the other intervals remaining within the expected error limits. In comparison, both the MOD09-based and Urban Clean peaks were approximately 0.85–0.90 and maintained stable A values across ranges, indicating robust control of systematic errors in the NIR band. Meanwhile, the LaSRC exhibited a sharp increase above 0.75 reflectance, exceeding the expected error threshold.

Regarding to P values, MOD04-based, MOD09-based, and Urban Clean all showed a monotonically increasing trend, exceeding the expected error limits when the SR surpassed 0.80. The MOD04-based type, in particular, showed relatively higher P values in the high-reflectance ranges, suggesting significant random errors. MOD09-based performs similarly to Urban Clean, with a slight advantage over Urban Clean in some ranges (0.55–0.75). LaSRC exhibits distinct interval-based characteristics. The P values were lower than those of the other algorithms in the low-reflectance range (0.15–0.45), indicating relatively small random errors. However, the P values rise sharply beyond the 0.6–0.65, exceeding the error threshold, but then become the lowest in high-reflectance regions (above 0.85), where random errors are well controlled.

The U values of MOD04-based, MOD09-based, and Urban Clean followed a similar trend, displaying small peaks at medium (~0.60) and high (~0.90) reflectance levels, surpassing the expected error limits when the SR exceeded 0.85. This indicates that the overall error increased for these three methods in the medium-to high-reflectance range. In contrast, LaSRC demonstrated a distinct monotonic increase in U values, exceeding the expected error limits over a wide range (above 0.6) and considerably higher than those of the other three methods, revealing notable deficiencies in the control of both random and systematic errors.

Overall, the findings for the NIR bands were consistent with those for the VIS bands. The MOD04-based type demonstrated superior performance in low-to-medium reflectance regions with the lowest A, P, and U values. The MOD09-based type effectively controlled systematic and random errors in bright surface regions, whereas Urban Clean achieved the lowest A, P, and U values at SR levels of approximately 0.5 and 0.8. LaSRC exhibited relatively low errors only within a certain low-reflectance range of the NIR bands.

SWIR bands: The A, P, and U values of the four products remained more stable in the SWIR bands than in the other bands. In general, the A, P, and U values exhibited a slow upward trend with increasing SR while remaining within the expected error range. This indicates that the processing methods for the SWIR bands can effectively control the errors under different reflectance conditions, particularly in the high-reflectance range.

https://doi.org/10.5194/egusphere-2026-1320
Preprint. Discussion started: 7 April 2026

For the A values, the MOD04-based, MOD09-based, and Urban Clean types exhibited similar trends, with a distinct trough around an SR of 0.3, indicating smaller systematic errors in low-reflectance regions. In contrast, the A-value curve from LaSRC remained relatively flat, suggesting more stable systematic errors, particularly in the high-reflectance ranges. Specifically, in Band 6, the MOD04-based type demonstrated outstanding performance in the low-reflectance range, with smaller systematic errors, whereas in the mid-to-high reflectance range, the Urban Clean type consistently maintained low systematic errors. In Band 7, although MOD09-based showed some advantages in the extremely low reflectance range (<0.1) and MOD04-based performed well in the low-reflectance region (0.1 – 0.4), LaSRC exhibited a superior ability to control systematic errors over a broader range, particularly in high-reflectance ranges.

The P-value trends of MOD04-based, MOD09-based, and Urban Clean show notable similarity, with distinct peaks emerging in the 0.35–0.40 and 0.85–0.90 reflectance ranges. These peaks indicate increased random errors and reduced error control capabilities within these intervals. In contrast, LaSRC demonstrated more stable P-value curves with minimal random errors and the lowest data dispersion at low reflectance levels (<0.3).

The U-value curves exhibited morphological similarities to the P-value curves across all four products, demonstrating a gradual decline in overall accuracy as SR increased, accompanied by two minor peaks in the U-value curves. For Band 6, MOD04-based showed a relative advantage only within the 0–0.1 reflectance range, while Urban Clean achieved superior performance in moderate-to-high reflectance intervals (0.45–0.85), exhibiting the smallest random errors and higher overall accuracy. LaSRC excels in low-reflectance ranges (0.1 – 0.45) with minimal errors and the lowest data dispersion. For Band 7, LaSRC outperformed all other products across all reflectance ranges, particularly in the bright surface regions, where its retrieval accuracy was significantly higher, highlighting its exceptional performance in SWIR-band retrieval.

Overall, in SWIR Band 6, each product exhibits distinct advantages at specific reflectance intervals. MOD04-based and MOD09-based types performed well in the 0–0.1 and 0.85–1.0 ranges, while Urban Clean excelled in the mid-to-high reflectance region, exhibiting the lowest random errors. LaSRC stands out in the low-reflectance range, demonstrating a lower uncertainty. For Band 7, LaSRC consistently outperformed the other algorithms across all SR intervals at the 2.1 μm wavelength, exhibiting the lowest overall error.

The following conclusions were drawn from the aforementioned analysis of SR results across different aerosol types, spectral bands, and reflectance intervals: The MOD04-based type exhibited smaller errors and higher overall accuracy in the visible and near-infrared (VNIR) bands; MOD09-based demonstrated superior performance in the high-reflectance ranges of the first six spectral bands with minimized errors; LaSRC showed notable superiority in the SWIR bands, particularly in Band 7 (2.1 μm), where both random and systematic errors were markedly lower than the other three products; while the Urban Clean type achieved high accuracy only in medium-reflectance regions near 1.6 μm (Band 6) but underperformed in other scenarios.

https://doi.org/10.5194/egusphere-2026-1320
Preprint. Discussion started: 7 April 2026

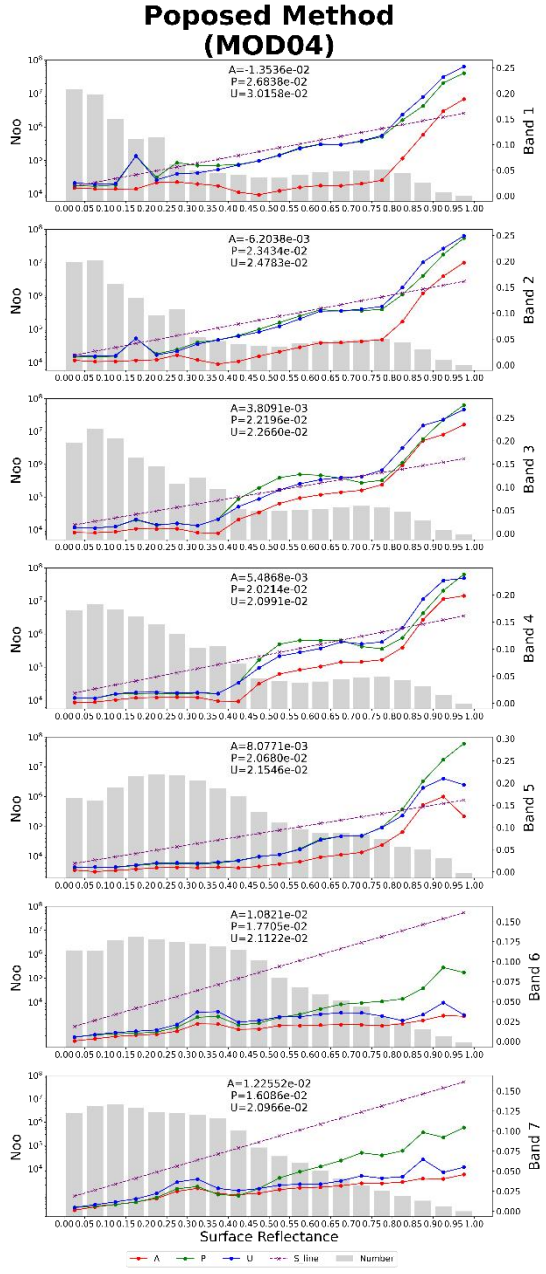

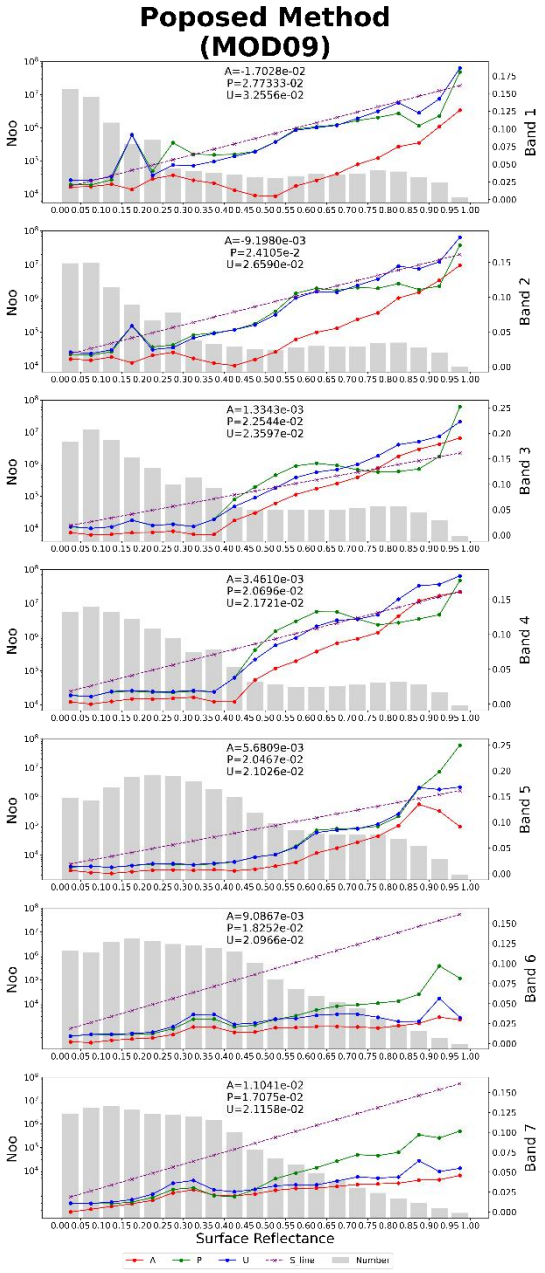

https://doi.org/10.5194/egusphere-2026-1320
Preprint. Discussion started: 7 April 2026

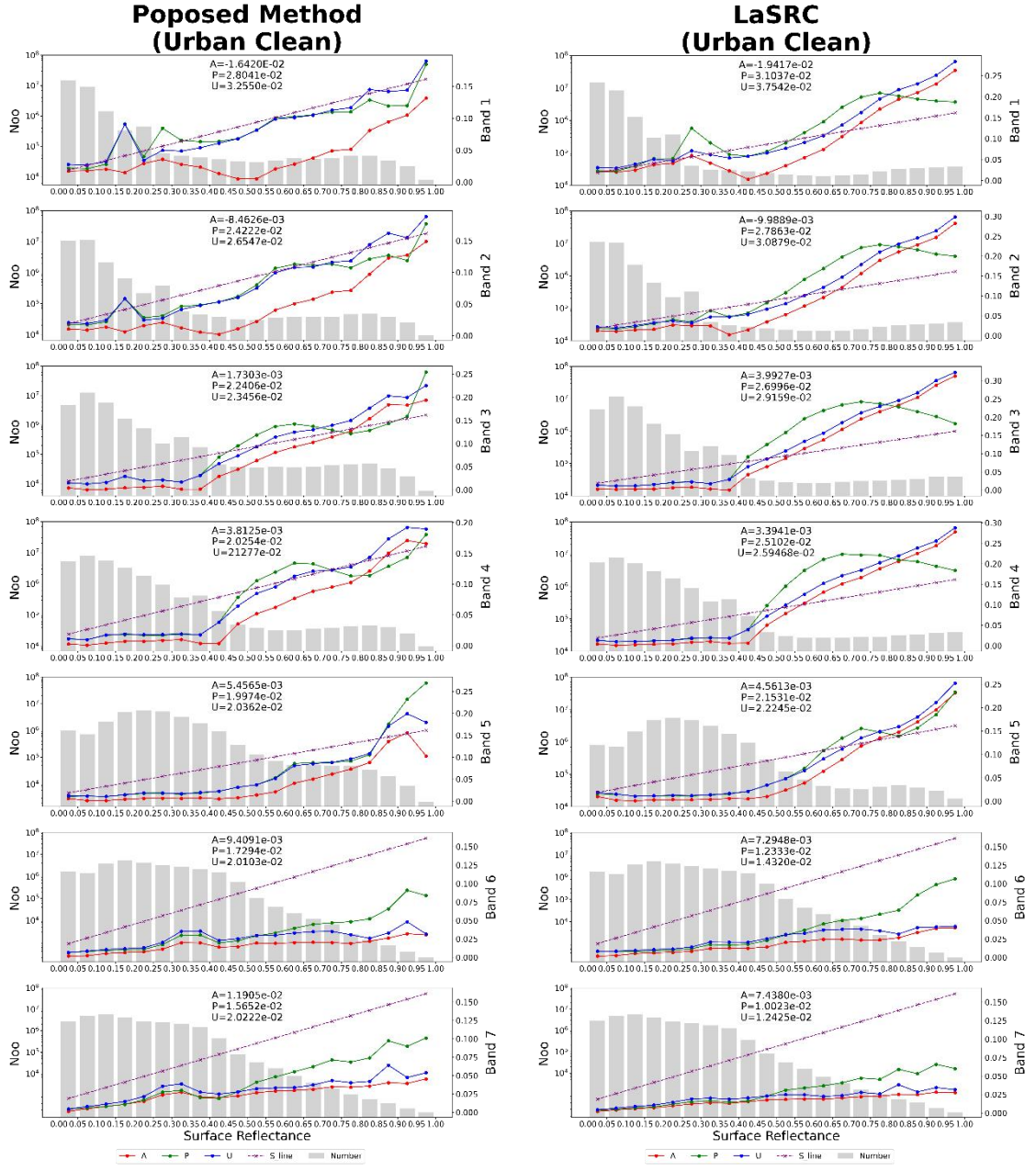

Figure 7: A, P, and U (y left axis) and the number of pixels (y right axis) of the four surface reflectance products within the 0.1 Surface Reflectance Range.

4) **Landcover SR assessment**

To evaluate the SR accuracy for different land surface types, multiple imagery scenes were randomly selected, and corresponding pixels for each surface type were extracted using RSEI, ensuring more than 5,000 sample points per type. The performance of the four SR products was assessed using RMSE and Bias across seven spectral bands, as shown in Fig. 8–9.

https://doi.org/10.5194/egusphere-2026-1320
Preprint. Discussion started: 7 April 2026

Overall, the SR retrieval performance exhibits distinct spectral behaviors across different surface types. Snow and vegetation generally show improved accuracy toward longer wavelengths, with errors notably reduced outside the short-wavelength region. Soil demonstrates relatively stable performance across the spectrum, with consistently low error levels. Building surfaces present moderate accuracy with slight spectral variability but without a clear monotonic trend. In contrast, water surfaces show a continuous improvement in retrieval accuracy toward longer wavelengths, with noticeably reduced errors in the SWIR region.

Bias analysis further reveals strong reflectance-dependent characteristics. High-reflectance surfaces (building and snow) tend to exhibit positive Bias values in longer wavelengths, indicating overestimation. Low-reflectance surfaces (soil, vegetation, and water) are predominantly underestimated in the VIS bands, although the magnitude and sign of Bias vary across wavelengths and products. The detailed comparisons for each surface type are discussed below.

Building: Building surfaces show moderate retrieval errors across bands, with RMSE reaching minimum values around Bands 3–4 and increasing again toward longer wavelengths. Among the four products, MOD04-based consistently achieves the lowest RMSE in Bands 1–4, demonstrating clear advantages in this region. In contrast, LaSRC shows larger RMSE in the VIS bands but becomes comparable to other products in Bands 5–7. MOD09-based exhibits the largest RMSE in Bands 1–2 but improves in the SWIR region. Urban Clean generally maintains intermediate performance across all bands.

Bias results indicate that all products exhibit wavelength-dependent transitions. Underestimation dominates in Bands 1–2, while overestimation becomes evident from Band 3 onward. MOD04-based maintains relatively smaller Bias magnitudes in most bands, whereas Urban Clean and LaSRC show larger positive Bias in the SWIR bands.

Snow: Snow surfaces exhibit relatively large retrieval errors in the VNIR region compared with their performance at longer wavelengths. RMSE values peak around Bands 2–4 and decrease rapidly toward Bands 6–7. MOD04-based achieves the lowest RMSE across nearly all bands, indicating the most stable performance over snow surfaces. MOD09-based produces significantly higher RMSE in Bands 1–5, suggesting reduced reliability in high-reflectance VNIR regions. Urban Clean and LaSRC show comparable performance in most bands, with slightly outperforming others in Band 7.

Bias values for snow are predominantly positive across all bands, indicating systematic overestimation. The magnitude of Bias peaks in Bands 2–4 and decreases substantially toward longer wavelengths. MOD04-based generally exhibits the smallest Bias across most bands, while MOD09-based shows the largest positive Bias, especially in the VNIR bands.

Soil: Soil surfaces demonstrate the most stable SR retrieval performance across spectral bands. RMSE values decrease rapidly from Band 1 to Band 3 and remain relatively low afterward. Among the four products, Urban Clean achieves the lowest RMSE in most bands, particularly in Bands 3–7. MOD09-based performs slightly better than other products in Bands 3–5 but shows increased RMSE at longer wavelengths. MOD04-based exhibits consistently higher RMSE than the other three products, indicating reduced stability over soil surfaces.

Bias results show that soil is generally underestimated in the VIS bands, with Bias gradually increasing toward zero or slight overestimation in longer wavelengths. Urban Clean and LaSRC maintain Bias values closest to zero across most bands, while MOD04-based exhibits stronger underestimation in Bands 1–2.

https://doi.org/10.5194/egusphere-2026-1320
Preprint. Discussion started: 7 April 2026

Vegetation: Vegetation surfaces show high RMSE in Band 1, followed by a sharp decrease toward Band 3 and relatively stable performance thereafter. MOD04-based achieves the lowest RMSE in Bands 1–2, demonstrating superior performance in short wavelengths. Urban Clean consistently provides the lowest RMSE from Bands 4–7, indicating advantages in NIR and SWIR regions. MOD09-based and LaSRC show comparable performance in Bands 3–5 but exhibit slightly higher RMSE in longer wavelengths.

Bias results indicate strong underestimation in Bands 1–2 for all products. The Bias gradually approaches zero or slightly positive values in longer wavelengths. Urban Clean maintains Bias values closest to zero in most bands, while LaSRC shows slightly larger positive Bias in Bands 5–7.

Water: Water surfaces exhibit decreasing retrieval accuracy with increasing wavelength. RMSE values are lowest in Bands 6–7 for most products, but VIS bands still demonstrate relatively strong performance compared with other surface types. MOD04-based achieves the lowest RMSE in Bands 1–4, indicating strong capability in VIS retrieval over water. Urban Clean performs best in Bands 5–7, achieving the smallest RMSE in the SWIR region. MOD09-based shows significantly higher RMSE in Bands 1–3, while LaSRC demonstrates relatively stable but slightly higher RMSE across most bands.

Bias analysis shows strong underestimation in Bands 1–3 for all products. The Bias magnitude decreases toward longer wavelengths, approaching near-zero values in Bands 6–7. MOD04-based generally maintains smaller Bias magnitudes in the VIS bands, whereas Urban Clean exhibits the lowest Bias in longer wavelengths.

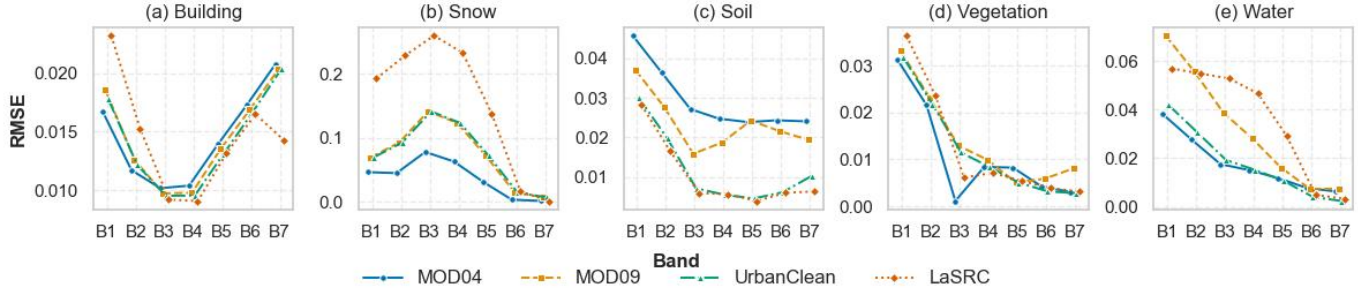

Figure 8: Scatter Plot of Measured vs. 6S-Simulated SR over Building-Surface .

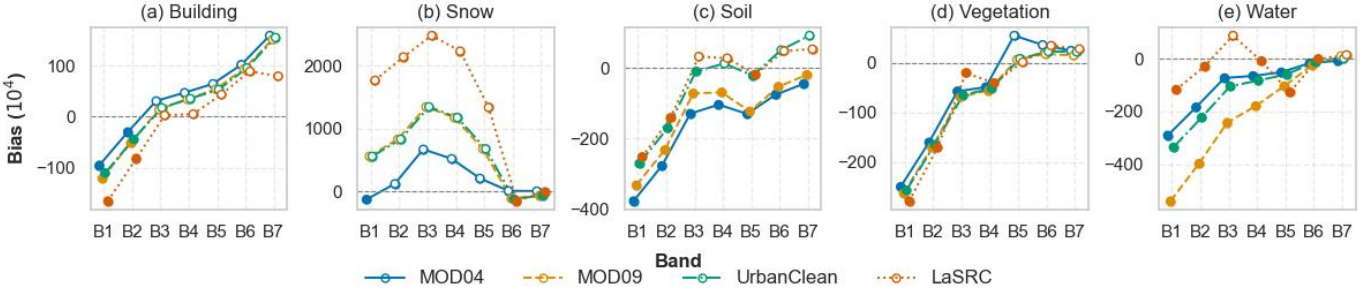

Figure 9: Scatter Plot of Measured vs. 6S-Simulated SR over Snow-Surface .

https://doi.org/10.5194/egusphere-2026-1320
Preprint. Discussion started: 7 April 2026

5 Discussions

5.1 AOD retrievals

In general, MOD04-based type demonstrated the best performance for AOD retrieval, yielding results closest to the actual observations.

Among the three aerosol types, the MOD04-based type had the highest R^2_AerT (0.7236), lowest bias (0.0052), and lowest RMSE (0.0437). This indicates a minimal deviation from the regression line, with the retrieved values closely matching site observations. The MOD09-based and Urban Clean exhibited similar scatter distributions, but Urban Clean had a lower Bias (0.0106) and RMSE (0.0548), and a higher R^2_AerT (0.5653), indicating that its deviations were generally smaller than those of the MOD09-based type and their retrieval values were more accurate. In contract, MOD09-based sample points were more dispersed. Furthermore, the results of the significance tests provide substantiation for the preceding findings. For both RMSE and bias, the differences among the three types were statistically significant, with MOD04-based demonstrating the best performance and MOD09-based the worst. While the R^2_AerT comparisons did not yield statistically significant differences, the observed mean differences were consistent with the overall performance ranking. The consistency between the effect size patterns and the point estimates supports the robustness of our conclusion.

As for the parameters of regression line, the MOD04-based type exhibits the smallest least-squares regression slope (0.9047). A threshold effect was observed; MOD04-based underestimated the optical depth above 0.15 and overestimated it below, with errors growing as AOD diverged further from the threshold. In comparison, the MOD09-based type showed a regression slope greater than 1 and a positive intercept, indicating a systematic AOD overestimation that intensified with increasing optical depth. Among the three types, Urban Clean exhibited a regression slope closest to 1 and an intercept near zero, indicating minimal systematic bias and well-balanced alignment of the sample points along the 1:1 reference line.

Furthermore, we assessed the uncertainty of the results, defining the uncertainty range as $0.15 \times AOD_{550}+0.05$, shown as a solid black line in Fig. 5. Among the three types, the MOD04-based type had the highest proportion of points within the uncertainty range (408 points), suggesting that its bias remained closer to the expected error thresholds and yielded more reliable results. Among the remaining two types, Urban Clean showed a superior performance, with a greater number of its points falling within the defined threshold (379 vs 349 points).

In conclusion, AOD retrievals using MOD04-based types generally have a higher accuracy than retrievals using other aerosol types. This may be attributed to the fact that MOD04-based refines aerosol type selection based on seasonality and geographic location, enabling the choice of aerosol types that better reflect local atmospheric conditions and thus improving AOD retrieval accuracy. In contrast, MOD09-based type determines subtypes solely by minimizing residuals without considering actual surface conditions. This approach resulted in a more dispersed sample distribution and an overall overestimation of the AOD. Urban Clean aerosol type employed in the LaSRC algorithm did not exhibit a notable advantage in AOD retrieval, probably because of its singular classification, which limits its applicability under diverse aerosol conditions. Consequently, the retrieval results tend to deviate more from the actual data. Nonetheless, the scattered degree of

https://doi.org/10.5194/egusphere-2026-1320
Preprint. Discussion started: 7 April 2026

dispersion in AOD for this single-type approach was lower than that of the MOD09-based approach, which incorporated five aerosol subtypes.

5.2 SR retrievals

Based on the validation results and preliminary conclusions across the four SR products under different spectral bands and full-range reflectance intervals, we conducted an in-depth investigation of the underlying causes of performance disparities during SR inversion. Leveraging the validation data from Fig. 7, the analysis primarily investigated performance discrepancies among the products, focusing on variations across spectral bands and reflectance intervals, while also assessing their similarities.

1) **Similar trends**

The vertical analysis in Fig. 7 reveals consistent trends in the accuracy metrics (A, P, and U) across all four products, with the performance declining from the VIS to SWIR bands. Notably, the SR accuracy improved with increasing wavelengths. In the VNIR bands, the A, P, and U values sharply increased, exceeding the error thresholds, particularly in the deep blue and blue bands, where the metrics peaked. By contrast, the accuracy of the SWIR bands remained within the expected error limit. These trends may be attributed to the wavelength-dependent aerosol effects. Shorter wavelengths, such as deep blue and blue wavelengths, are more sensitive to AOD and amplify the retrieval errors. Additionally, simplified aerosol-type assumptions in retrieval algorithms may increase the uncertainties in low-reflectance areas. Conversely, reduced atmospheric scattering and absorption in the SWIR bands led to more stable inversion and improved precision.

Horizontal analysis showed a systematic increase in the A, P, and U values with higher SR across all products (Fig. 7), indicating reduced accuracy at high reflectance. In high-reflectance cases (e.g., snow and clouds), all methods exceeded predefined error thresholds, likely owing to limitations in AC models for highly reflective surfaces. Overamplification of the surface signals in these scenarios introduces nonlinear errors, further reducing the retrieval accuracy.

2) **Different performance**

The validation results revealed distinct performance variations among the four SR products.

MOD04-based: The MOD04-based type demonstrated superior retrieval accuracy in the VNIR bands across moderate-to-low reflectance ranges, outperforming the other products. This advantage is likely due to the incorporation of region- and season-specific aerosol parameters, which enhance adaptability to spatiotemporal environmental variations. Because medium-to-low reflectance pixels account for a high proportion of most remote sensing images, MOD04-based type is applicable to most scenes and enable high-precision surface-reflectance inversion. The strength of this type lies in its capacity to balance aerosol subtype characterization with spatiotemporal variability, thereby minimizing systematic biases under complex atmospheric conditions.

In summary, the MOD04-based type demonstrated exceptional inversion accuracy and generalizability in the VNIR bands under moderate-to-low reflectance scenarios, which can be attributed to its comprehensive consideration of the geographic and seasonal aerosol dynamics. This capability makes it a reliable reference for SR retrieval with broad potential for global-

https://doi.org/10.5194/egusphere-2026-1320
Preprint. Discussion started: 7 April 2026

scale AC applications in the future.

MOD09-based: The validation results indicated that the SR product corresponding to the MOD09-based aerosol type performed exceptionally well in a relatively narrow high-reflectance range (>0.8). Across the first six bands examined in this study, although the errors for all four products exceeded the acceptable range in this interval, the MOD09-based type effectively controlled these errors and demonstrated a superior retrieval accuracy. This advantage can be attributed to the application of residual constraints during AOD retrieval, which enables effective error regulation, thereby improving the SR retrieval accuracy in high-reflectance ranges, particularly in remote sensing imagery of large-scale high-reflectance surfaces (e.g., snow). However, the introduction of residual constraints may cause abrupt changes in the subtypes of adjacent pixels that are not entirely consistent with gradual spatial variation in aerosols. We applied an overall smoothing process to AOD results to mitigate the uncertainty introduced by these abrupt changes. However, this approach has inherent limitations, and may not eliminate the effects of abrupt transitions arising from subtype selection. Consequently, future research should aim to enhance the spatial continuity of aerosol retrieval by investigating more appropriate smoothing strategies or alternative adjustment methods to minimize the potential adverse effects of these abrupt transitions on AOD and SR retrieval accuracies. In conclusion, despite the exceptional performance of the MOD09-based aerosol type in high-reflectance ranges, making it a valuable tool for processing remote sensing images with extreme SR conditions, its subtype selection method under residual constraints is associated with certain risks.

Urban Clean: Among the four SR products, the Urban Clean aerosol type, a subtype integrated into the LaSRC algorithm, exhibited the weakest overall performance. It demonstrates limited advantages only at specific intervals, such as the moderate reflectance ranges in band 6, with generally inferior inversion accuracy compared with other products. Its error patterns partially align with the MOD09-based aerosol type but remain systematically less robust. This underperformance likely stems from the specialized design as a subtype of the MOD09-based design, which is optimized for urban areas with low air quality and stringent application constraints. Consequently, their narrow applicability limits their global utility, particularly in heterogeneous environments.

In summary, although Urban Clean shows localized efficacy, its restricted operational scope and demanding implementation criteria render it non-competitive with other types of global SR inversion tasks.

LaSRC product: The LaSRC product demonstrated marked superiority in the SWIR bands, especially in Band 7 (2.1 μm), where its SR estimates exhibited enhanced precision and reliability. This advantage is amplified with increasing reflectance levels, which is likely attributable to the refined handling of water vapor and other absorptive gases that critically influence the SWIR bands. The LaSRC algorithm effectively mitigates atmospheric interference, enabling high-fidelity retrieval in these spectral ranges. Notably, its performance surpassed that of the other products in high-reflectance SWIR scenarios.

However, LaSRC exhibits elevated error levels in the VNIR bands. The A-value (systematic bias) consistently exceeded that of the other products, suggesting pronounced deviations. This discrepancy may originate from (1) the residual quality control method used in LaSRC, which flags pixels failing band 4/5/7 spectral tests as water bodies, potentially propagating AOD retrieval errors into VNIR reflectance estimates, and (2) the atmospheric parameters in the LaSRC method interpolated using

https://doi.org/10.5194/egusphere-2026-1320
Preprint. Discussion started: 7 April 2026

AOD via cubic spline functions, which may introduce errors.

In conclusion, although the excellent performance of LaSRC in the SWIR band highlights its potential for high-precision reflectance retrieval, its systematic VNIR errors require further investigation to guide the refinement of algorithms.

These comparisons revealed the underlying factors contributing to the differences in product performance, such as the adaptability of MOD04-based aerosol parameterization. These insights offer practical guidance for optimizing the selection of dynamic aerosol types based on scene characteristics and highlight the potential advantage of the LaSRC algorithm in improving reflectance accuracy through a more effective correction of absorptive gas effects.

3) **SR retrievals with different landcover**

Fig. 8–9 indicate that SR retrieval accuracy exhibits clear spectral dependence that varies with surface type. For snow and vegetation, retrieval errors are generally larger in shorter wavelengths and decrease toward longer wavelengths, which is consistent with the stronger influence of aerosol scattering in the VIS region. Soil shows relatively stable performance across spectral bands, while water exhibits a distinct spectral behavior, with retrieval accuracy improving toward longer wavelengths. These variations reflect the combined effects of aerosol scattering, gaseous absorption, and surface reflectance characteristics.

For soil surfaces, SR retrievals show relatively stable spectral behavior. Soil spectra typically vary smoothly with wavelength and often exhibit comparatively homogeneous spatial distributions. Although soil reflectance is influenced by mineral composition, organic matter, and moisture content, these factors usually introduce gradual spectral variations, which favor stable atmospheric correction performance.

Among the four products, LaSRC shows strong performance for soil pixels, while the single-aerosol-type products (Urban Clean and LaSRC) generally demonstrate stable behavior across multiple spectral bands. The use of a single aerosol type reduces uncertainties associated with aerosol subtype selection and provides a more consistent atmospheric correction baseline. Such stability is particularly beneficial for surfaces with relatively smooth spectral signatures and weaker atmospheric coupling, such as soil.

For vegetation and building surfaces, retrieval performance is strongly influenced by surface complexity. Vegetation canopies consist of multilayer structures, while urban areas contain diverse materials and complex geometric configurations. These characteristics enhance BRDF effects, mixed pixels, and shadowing, thereby increasing atmospheric correction uncertainty. MOD04-based shows advantages in the deep blue and blue bands, which may be related to its aerosol subtype selection scheme that incorporates seasonal and geographic variability. By better representing aerosol optical properties, this approach may improve retrieval robustness in spectrally sensitive short-wavelength regions. In contrast, MOD09-based relies primarily on an error-minimization strategy for subtype selection, which may occasionally reduce physical consistency and introduce additional uncertainties over spectrally complex surfaces.

Urban Clean and LaSRC show relatively stable performance in the NIR and SWIR regions. As aerosol scattering effects weaken with increasing wavelength, atmospheric correction becomes less sensitive to aerosol-type selection, allowing systematic model assumptions to be more effectively compensated during retrieval. In contrast, multi-subtype selection

https://doi.org/10.5194/egusphere-2026-1320
Preprint. Discussion started: 7 April 2026

strategies used in MOD04-based and MOD09-based may introduce additional variability when aerosol sensitivity is reduced. For water and snow surfaces, SR retrieval is strongly affected by their extreme reflectance characteristics. Water surfaces are characterized by very low reflectance, strong gaseous absorption, and additional variability caused by surface roughness and specular reflection, all of which increase retrieval uncertainty. Snow surfaces, on the other hand, exhibit extremely high reflectance in the VIS region, which may increase retrieval sensitivity and introduce systematic biases. In practical atmospheric correction implementations, aerosol properties over water and snow are often constrained by climatological assumptions, which may introduce additional systematic uncertainties. Among the four products, MOD04-based demonstrates stable performance over snow surfaces and in VIS bands for water pixels, likely benefiting from its physically constrained aerosol parameterization. Urban Clean shows advantages over water surfaces in longer wavelengths, reflecting its stability in spectral regions less sensitive to aerosol scattering. MOD09-based generally exhibits larger retrieval variability, possibly due to its heavy reliance on mathematical optimization without sufficient physical constraints. LaSRC demonstrates stable performance for soil surfaces and maintains competitive accuracy in longer wavelengths but shows relatively larger systematic deviations under extreme reflectance conditions.

Overall, the analysis suggests that aerosol treatment strategies play an important role in determining SR retrieval performance across surface types. Physically constrained aerosol schemes tend to provide improved robustness in short-wavelength regions, while simplified or single-type aerosol models provide stable performance in spectral regions where aerosol sensitivity is reduced.

5.3 Future Strategies

Based on the validation results for AOD and SR, the following operational guidelines were proposed for selecting the dynamic aerosol types (MOD04-based, MOD09-based, and Urban Clean):

a) MOD04-based aerosol type is recommended for AOD retrieval across extensive and topographically complex regions. Its adaptive parameterization scheme, which incorporates seasonal- and geographical-dependent aerosol properties, ensures better alignment with surface typologies, thereby delivering higher retrieval accuracy. However, the MOD04-based type may systematically overestimate AOD in scenes with high AOD levels. To mitigate this bias, global linear correction should be implemented for such datasets to enhance the reliability of the results.

b) When retrieving SR data from commonly used VNIR four-band remote sensing imagery such as China's Gaofen-1 (Lu et al., 2015) and Gaofen-2 (Huang et al., 2018), we recommend using the MOD04-based dynamic aerosol type. This type exhibited higher retrieval accuracy for medium- to low-reflectance pixels in the VNIR bands. Given the predominance of such pixels in remote-sensing imagery, the MOD04-based type offers notable advantages for surface-reflectance retrieval in VNIR applications.

c) When retrieving SR data from remote sensing imagery containing extensive high-reflectance terrain features, we recommend using the MOD09-based dynamic aerosol type. This approach employs the residual minimization principle to constrain errors, and demonstrates superior performance in the inversion of high-reflectance surfaces. In particular, for

https://doi.org/10.5194/egusphere-2026-1320
Preprint. Discussion started: 7 April 2026

extensive high-reflectance features such as snow-covered areas and urban structures, the MOD09-based type effectively enhances the inversion accuracy and provides more reliable SR estimates.

The following recommendations were proposed for LaSRC products: In remote sensing applications that rely on SWIR bands, such as snow/ice detection and land-cover change monitoring, the LaSRC product should be prioritized as the data source. Its higher accuracy in the SWIR-band SR estimation provides more reliable spectral information, thereby enhancing the scientific validity and operational reliability of related applications.

It is worth noting that, while our recommendations are derived under relatively homogeneous atmospheric conditions, the complex variability of real-world environments means they should only serve as one criterion for aerosol type selection. In practical applications, users should combine multiple indicators and data-driven considerations to make final choices.

Table 7. Performance summary of four models for AOD and SR retrieval.

	MOD04-based	MOD09-based	Urban Clean	LaSRC
AOD retrieval	Best	Lower	Moderate	-
SR retrieval	Best in VNIR	Best in high-reflectance	Similar to MOD09-based, slightly worse	Best in SWIR
SR by land cover type	Water, snow	normal	Vegetation, building	Vegetation, building

6 Conclusions

This study derived AOD and SR data from Landsat 8 imagery across 100 global sites for the year 2022 through AC using three dynamic aerosol types (MOD04-based, MOD09-based, and Urban Clean).

The results were validated against ground truth measurements. For AOD evaluation, a comparative analysis of three aerosol treatment strategies was conducted using linear regression analysis and accuracy metrics, demonstrating the strong performance of the MOD04-based type. In the comparative analysis of SR products, the official Landsat 8 LaSRC product was included, and the accuracy of four SR products was evaluated across the full reflectance range using three performance metrics (A, P, and U). The validation results indicate that the MOD04-based type achieved high retrieval accuracy in the VNIR spectral bands. The MOD09-based type demonstrated relatively strong performance in high-reflectance conditions. The Urban Clean type yielded performance comparable to MOD09-based in certain reflectance ranges but showed limited advantages overall. The LaSRC product exhibited clear strengths in the SWIR region, particularly around 2.1 μm, while maintaining competitive performance in other bands.

The land cover–based analysis reveals that SR retrieval performance varies with surface spectral characteristics and structural complexity. For soil surfaces, LaSRC demonstrates strong performance across spectral bands. For vegetation and building surfaces, Urban Clean shows stable behavior in the NIR region, while MOD04-based provides improved performance in the deep-blue and blue bands. For water and snow surfaces, MOD04-based demonstrates stable performance

https://doi.org/10.5194/egusphere-2026-1320
Preprint. Discussion started: 7 April 2026

in the VIS bands, whereas Urban Clean shows advantages in longer wavelengths. MOD09-based generally exhibits larger retrieval variability across surface conditions.

The analyses from the perspectives of performance metrics and land cover types exhibit both consistency and complementarity. Both approaches reveal similar spectral performance patterns, such as the strong VIS-band performance of MOD04-based and the SWIR advantages of LaSRC. Meanwhile, the land cover–based evaluation highlights the influence of surface characteristics on retrieval behavior. For example, Urban Clean shows relatively stable performance in the NIR region for vegetation and building surfaces. In contrast, MOD09-based demonstrates greater variability across reflectance conditions, and its advantages in high-reflectance conditions are not consistently observed across different surface environments. These results suggest that SR retrieval performance is influenced by the combined effects of spectral characteristics, reflectance magnitude, and surface structure. The agreement and divergence between the two evaluation perspectives provide a more comprehensive understanding of retrieval performance.

Notably, the current conclusions were derived from existing sites and datasets. In practical applications, a more in-depth analysis and specific processing are required, considering diverse scenarios and image characteristics. In addition, the present study utilized only one year of remote sensing data, which provides valuable insights but may limit the generalizability of the conclusions. Therefore, subsequent studies should expand the validation not only to additional geographical regions and land cover types but also to multi-year datasets, thereby capturing seasonal and interannual variations. By increasing the sample size and data diversity, we aimed to rigorously assess aerosol-type performance across various environmental conditions thereby enhancing its global applicability and reliability.

Furthermore, the observed superiority of the LaSRC algorithm in the SWIR bands, particularly near 2.1 μm, warrants mechanistic investigation. Future studies should focus on elucidating the physical and algorithmic foundations of these advantages. Through targeted optimization of LaSRC SWIR-band reflectance retrieval workflows, we sought to advance the accuracy of large-scale surface monitoring and explore its broader application potential in multi-sensor remote sensing.

Code and data availability

The code used in this study is not publicly available due to commercial considerations. The datasets used in this work are publicly available remote sensing and ground-based observation products. Satellite data were obtained from the Landsat 8 mission provided by the United States Geological Survey (USGS) Earth Resources Observation and Science (EROS) Center. Aerosol optical depth data were obtained from the Aerosol Robotic Network (AERONET) database. These datasets can be accessed through the official USGS and AERONET websites. Further information about the datasets used in this study can be provided by the authors upon reasonable request.

https://doi.org/10.5194/egusphere-2026-1320
Preprint. Discussion started: 7 April 2026

Author contributions

Shuning Zhang conducted the experiments and wrote the manuscript. Hao Zhang designed the study and provided supervision. Bing Zhang contributed to the scientific guidance of the study. Zhenzhen Cui performed the data preprocessing. All authors reviewed and approved the final manuscript.

Competing interests

The authors declare that they have no conflict of interest.

Acknowledgements

The authors acknowledge the U.S. Geological Survey (USGS) for providing the Landsat 8 surface reflectance data and the NASA Goddard Space Flight Center and the contributing principal investigators for the AERONET data used in this study. The authors would also like to express their sincere gratitude to the anonymous reviewers for their constructive comments and suggestions, which greatly helped improve the quality and clarity of this manuscript.

Financial support

This work was supported by the Deep Earth Probe and Mineral Resources Exploration - National Science and Technology Major Project of China(2024ZD1002100) and the National Natural Science Foundation of China (41771397).

References

Ångström, A.: The parameters of atmospheric turbidity, Tellus, 16, 64–75, 1964.

Anderson, G. P., Pukall, B., Allred, C. L., Jeong, L. S., Hoke, L. M., Chetwynd, J. H., Adler-Golden, S. M., Berk, A., Bernstein, L. S., Bernstein, S. C., Acharya, P. K., and Matthew, W. M.: FLAASH and MODTRAN4: state-of-the-art atmospheric correction for hyperspectral data, 1999 IEEE Aerosp. Conf. Proc., 4, 177–181, 1999.

Berk, A., Bosch, J., Hawes, F., Perkins, T., Conforti, P. F., Anderson, G. P., Kennett, R. G., and Acharya, P. K.: MODTRAN® 6.0 User's Manual, Air Force Res. Lab., 2018.

Brazile, J., Richter, R., Schläpfer, D., Schaepman, M. E., and Itten, K. I.: Cluster versus grid for operational MODTRAN-based look-up table generation of ATCOR tables, Parallel Comput., 34, 32–46, 2008.

Chen, L., Wang, R., Fei, Y., Fang, P., Zha, Y., and Chen, H.: Multi-angle aerosol optical depth retrieval method based on improved surface reflectance, Atmos. Meas. Tech., 17, 4411–4430, https://doi.org/10.5194/amt-17-4411-2024, 2024.

https://doi.org/10.5194/egusphere-2026-1320
Preprint. Discussion started: 7 April 2026

Lu, C., and Bai, Z.: Characteristics and typical applications of GF-1 satellite, 2015 IEEE Int. Geosci. Remote Sens. Symp. (IGARSS), 1246–1249, 2015.

Doxani, G., Vermote, E. F., Roger, G. C., Skakun, S., Gascon, F., Collison, A., Keukelaere, L. D., Desjardins, C., Frantz, D., Hagolle, O., Kim, M., Louis, J., Pacifici, F., Pflug, B., Poilvé, H., Ramon, D., Richter, R., and Yin, F.: Atmospheric correction inter-comparison exercise (ACIX-II Land): An assessment of atmospheric correction processors for Landsat-8 and Sentinel-2 over land, Remote Sens. Environ., 285, 113412, 2023.

Dubovik, O., Smirnov, A., Holben, B. N., King, M. D., Kaufman, Y. J., Eck, T. F., and Slutsker, I.: Accuracy assessments of aerosol optical properties retrieved from Aerosol Robotic Network (AERONET) Sun and sky radiance measurements, J. Geophys. Res. Atmos., 105, 9791–9806, 2000.

Dubovik, O., Holben, B. N., Eck, T. F., Smirnov, A., Kaufman, Y. J., King, M. D., Tanré, D., and Slutsker, I.: Variability of absorption and optical properties of key aerosol types observed in worldwide locations, J. Atmos. Sci., 59, 590–608, 2002.

Dwyer, J. L., Roy, D. P., Sauer, B., Jenkerson, C. B., Zhang, H. K., and Lymburner, L.: Analysis ready data: enabling analysis of the Landsat archive, Remote Sens., 10, 1363, 2018.

Eck, T. F., Holben, B. N., Reid, J. S., O'Neill, N. T., Schafer, J. S., Dubovik, O., Smirnov, A., Yamasoe, M. A., and Artaxo, P.: High aerosol optical depth biomass burning events: a comparison of optical properties for different source regions, Geophys. Res. Lett., 30, 2003.

Friedl, M. A., McIver, D. K., Hodges, J. C. F., Zhang, X. Y., Muchoney, D., Strahler, A. H., Woodcock, C. E., Gopal, S., Schneider, A., Cooper, A., Baccini, A., Gao, F., and Schaaf, C.: Global land cover mapping from MODIS: algorithms and early results, Remote Sens. Environ., 83, 287–302, 2002.

Gao, B. C., Heidebrecht, K. B., and Goetz, A. F. H.: Atmospheric removal program (ATREM) user's guide, Center Study Earth Space, Univ. Colorado, Boulder, 1992.

Gathman, S. G.: Optical properties of the marine aerosol as predicted by a BASIC version of the Navy Aerosol Model, Naval Res. Lab. Rep., 1983.

Giles, D. M., Sinyuk, A., Sorokin, M. S., Schafer, J. S., Smirnov, A., Slutsker, I., Eck, T. F., Holben, B. N., Lewis, J., Campbell, J., Welton, E. J., Korkin, S., and Lyapustin, A.: Advancements in the Aerosol Robotic Network (AERONET) Version 3 database, Atmos. Meas. Tech., 12, 169–209, 2019.

Grey, W. M. F., North, P. R. J., Los, S. O., and Mitchell, R. M.: Aerosol optical depth and land surface reflectance from multi-angle AATSR measurements, IEEE Trans. Geosci. Remote Sens., 44, 2184–2197, 2006.

Guanter, L., Richter, R., and Kaufmann, H.: On the application of the MODTRAN4 atmospheric radiative transfer code to optical remote sensing, Int. J. Remote Sens., 30, 1407–1424, 2009.

Holben, B. N., Eck, T. F., Slutsker, I., Tanré, D., Buis, J. P., Setzer, A., Vermote, E. F., Reagan, J. A., Kaufman, Y. J., Nakajima, T., Lavenu, F., Jankowiak, I., and Smirnov, A.: AERONET – a federated instrument network and data archive for aerosol characterization, Remote Sens. Environ., 66, 1–16, 1998.

https://doi.org/10.5194/egusphere-2026-1320
Preprint. Discussion started: 7 April 2026

Hsu, N. C., Jeong, M. J., Bettenhausen, C., Sayer, A. M., Hansell, M., Seftor, C. S., Huang, J., and Tsay, S. C.: Enhanced Deep Blue aerosol retrieval algorithm: the second generation, J. Geophys. Res. Atmos., 118, 9296–9315, 2013.

Huang, W., Sun, S., Jiang, H., Gao, C., and Zong, X.: GF-2 satellite 1 m/4 m camera design and in-orbit commissioning, Chin. J. Electron., 27, 1316–1321, 2018.

Ichoku, C., Remer, L. A., Kaufman, Y. J., Levy, R., Chu, D. A., Tanré, D., and Holben, B. N.: MODIS observation of aerosols and estimation of aerosol radiative forcing over southern Africa during SAFARI 2000, J. Geophys. Res. Atmos., 108, 2003.

Kaufman, Y. J., Tanré, D., Remer, L. A., Vermote, E. F., Chu, A., and Holben, B. N.: Operational remote sensing of tropospheric aerosol over land from EOS moderate resolution imaging spectroradiometer, J. Geophys. Res. Atmos., 102, 17051–17067, 1997.

Levy, R. C., Remer, L. A., and Dubovik, O.: Global aerosol optical properties and application to Moderate Resolution Imaging Spectroradiometer aerosol retrieval over land, J. Geophys. Res. Atmos., 112, 2007a.

Levy, R. C., Remer, L. A., Mattoo, S., Vermote, E. F., and Kaufman, Y. J.: Second-generation operational algorithm: Retrieval of aerosol properties over land from inversion of Moderate Resolution Imaging Spectroradiometer spectral reflectance, J. Geophys. Res. Atmos., 112, 2007b.

Levy, R. C., Remer, L. A., Tanré, D., Kaufman, Y. J., Ichoku, C., Holben, B. N., Livingston, J. M., Russell, P. B., and Maring, H.: Evaluation of the Moderate Resolution Imaging Spectroradiometer (MODIS) retrievals of dust aerosol over the ocean during PRIDE, J. Geophys. Res. Atmos., 108, 2003.

Li, Z., Xu, H., Li, K. T., Li, D. H., Xie, Y. S., Li, L., Zhang, Y., Gu, X. F., Zhao, W., Tian, Q. J., Deng, R. R., Su, X. L., Huang, B., Qiao, Y. L., Cui, W. Y., Hu, Y., Gong, C. L., Wang, Y. Q., Wang, X. F., Wang, J. P., Du, W. B., Pan, Z. Q., Li, Z. Z., and Bu, D.: Comprehensive study of optical, physical, chemical, and radiative properties of total columnar atmospheric aerosols over China: An overview of Sun–Sky Radiometer Observation Network (SONET) measurements, Bull. Am. Meteorol. Soc., 99, 739–755, 2018.

Longtin, D. R., Shettle, E. P., Hummel, J. R., and Pryce, J. D.: A wind-dependent desert aerosol model: radiative properties, Air Force Geophys. Lab., 1988.

Lyapustin, A., Wang, Y., Korkin, S., and Huang, D.: MODIS collection 6 MAIAC algorithm, Atmos. Meas. Tech., 11, 5741–5765, 2018.

Lyapustin, A., Zhao, F., and Wang, Y.: A comparison of multi-angle implementation of atmospheric correction and MOD09 daily surface reflectance products from MODIS, Front. Remote Sens., 2, 712093, 2021.

Maciel, D. A., Pahlevan, N., Barbosa, C. C. F., Novo, E. M. L. M., Paulino, R. S., Martins, V. S., Vermote, E. F., and Crawford, C. J.: Validity of the Landsat surface reflectance archive for aquatic science: Implications for cloud ‐ based analysis, Limnol. Oceanogr. Lett., 8, 850–858, 2023.

https://doi.org/10.5194/egusphere-2026-1320
Preprint. Discussion started: 7 April 2026

Mann, J., Maddox, E., Shrestha, M., Irwin, J., Czapla-Myers, J., Gerace, A., Rehman, E., Raqueno, N., Coburn, C., Byrne, G., Broomhall, M., and Walsh, A.: Landsat-8 and 9 underfly international surface reflectance validation collaboration, Remote Sens., 16, 1492, 2024.

Masek, J. G., Vermote, E. F., Saleous, N. E., Wolfe, R., Hall, F. G., Huemmrich, K. F., Gao, F., Kutler, J., and Lim, T. K.: A Landsat surface reflectance dataset for North America 1990–2000, IEEE Geosci. Remote Sens. Lett., 3, 68–72, 2006.

Meghraj, K. C., Leigh, L., Pinto, C. T., and Kaewmanee, M.: Method of validating satellite surface reflectance product using empirical line method, Remote Sens., 15, 2240, 2023.

Miller, C. J.: Performance assessment of ACORN atmospheric correction algorithm, Proc. SPIE, 4725, 438–449, 2002.

Mueller-Wilm, U., Devignot, O., and Pessiot, L.: Sen2Cor configuration and user manual, ESA, 2017.

Pashayi, M., Satari, M., and Shahraki, M. M.: Multi-layer retrieval of aerosol optical depth in the troposphere using SEVIRI data, Atmos. Meas. Tech., 18, 1415–1439, https://doi.org/10.5194/amt-18-1415-2025, 2025.

Perkins, T., Adler-Golden, S., Cappelaere, P., and Mandl, D.: High-speed atmospheric correction for spectral image processing, Proc. SPIE, 8390, 246–252, 2012a.

Perkins, T., Adler-Golden, S., Matthew, M. W., Berk, A., Bernstein, L. S., Lee, J., and Fox, M.: Speed and accuracy improvements in FLAASH atmospheric correction of hyperspectral imagery, Opt. Eng., 51, 111707, 2012b.

Radosavljevic, V., Vucetic, S., and Obradovic, Z.: Aerosol optical depth retrieval by neural networks ensemble with adaptive cost function, Proc. 10th Int. Conf. Eng. Appl. Neural Netw., 266–275, 2007.

Remer, L. A., and Kaufman, Y. J.: Dynamic aerosol model: urban/industrial aerosol, J. Geophys. Res. Atmos., 103, 13859–13871, 1998.

Remer, L. A., Kaufman, Y. J., Tanré, D., Mattoo, S., Chu, D. A., Martins, J. V., Li, R. R., Ichoku, C., Levy, R. C., Kleidman, R. G., Eck, T. F., Vermote, E. F., and Holben, B. N.: The MODIS aerosol algorithm, products, and validation, J. Atmos. Sci., 62, 947–973, 2005.

Richter, R., Louis, J., Muller-Wilm, U., Laroque, C., and Dingeldey, C.: Sentinel-2 MSI Level 2A Products Algorithm Theoretical Basis Document Issue: 2.0, ESA, 2012.

Richter, R., and Schläpfer, D.: Atmospheric and topographic correction (ATCOR theoretical background document), DLR IB, 1, 0564–03, 2019.

Roy, D. P., Ju, J., Kline, K., Scaramuzza, P. L., Kovalskyy, V., Hansen, M., Loveland, T., Vermote, E. F., and Zhang, C.: Web-enabled Landsat Data (WELD): Landsat ETM+ composited mosaics of the conterminous United States, Remote Sens. Environ., 114, 35–49, 2010.

Roy, D. P., Wulder, M. A., Loveland, T. R., Woodcock, C. E., Allen, R. G., Anderson, M. C., Helder, D., Irons, J. R., Johnson, D. M., Kennedy, R., Scambos, T. A., Schaaf, C. B., Schott, J. R., Sheng, Y., Vermote, E. F., Belward, A. S., Bindschadler, R., Cohen, W. B., Gao, F., Hipple, J. D., Hostert, P., Huntington, J., Justice, C. O., Kilic, A., Kovalskyy, V., Lee, Z. P., Lymburner, L., Masek, J. G., McCorkel, J., Shuai, Y., Trezza, R., Vogelmann, J., Wynne, R. H., and Zhu, Z.: Landsat-8: science and product vision for terrestrial global change research, Remote Sens. Environ., 145, 154–172, 2014.

https://doi.org/10.5194/egusphere-2026-1320
Preprint. Discussion started: 7 April 2026

Satheesh, S. K., and Moorthy, K. K.: Radiative effects of natural aerosols: a review, Atmos. Environ., 39, 2089–2110, 2005.

Schläpfer, D., and Richter, R.: Geo-atmospheric processing of airborne imaging spectrometry data. Part 1: parametric orthorectification, Int. J. Remote Sens., 23, 2609–2630, 2002.

She, L., Li, Z., Leeuw, G., Wang, W., Wang, Y., Yang, L., Feng, Z., Yang, C., and Shi, Y.: Time series retrieval of multi-wavelength aerosol optical depth by adapting Transformer (TMAT) using Himawari-8 AHI data, Remote Sens. Environ., 305, 114115, https://doi.org/10.1016/j.rse.2024.114115, 2024.

She, L., Zhang, H. K., Bu, Z., Shi, Y., Yang, L., and Zhao, J.: A Deep-Neural-Network-Based Aerosol Optical Depth (AOD) Retrieval from Landsat-8 Top of Atmosphere Data, Remote Sens., 14, 1411, https://doi.org/10.3390/rs14061411, 2022.

Shettle, E. P., and Fenn, R. W.: Models for the Aerosols of the Lower Atmosphere and the Effects of Humidity Variations on Their Optical Properties, Air Force Geophys. Lab., 1979.

Staenz, K., and Williams, D.: Retrieval of surface reflectance from hyperspectral data using a look-up table approach, Can. J. Remote Sens., 23, 354–368, 1997.

Staenz, K., Szeredi, T., and Schwarz, J.: ISDAS – a system for processing and analyzing hyperspectral data, Can. J. Remote Sens., 24, 99–113, 1998.

Superczynski, S. D., Kondragunta, S., and Lyapustin, A. I.: Evaluation of the multi‐angle implementation of atmospheric correction (MAIAC) aerosol algorithm through intercomparison with VIIRS aerosol products and AERONET, J. Geophys. Res. Atmos., 122, 3005‐3022, 2017.

Takamura, T., Nakajima, T., and SKYNET Community Group: Overview of SKYNET and its activities, Opt. Pura Apl., 37, 3303–3308, 2004.

Toller, G., Isaacman, A., Kuyper, J., and Toller, G.: MODIS Level 1B Product User's Guide for Level 1B Version 6.1.0 (Terra) and Version 6.1.1 (Aqua), NASA MCST, 2009.

Vermote, E. F., Tanré, D., Deuze, J. L., Herman, M., and Morcrette, J. J.: Second Simulation of a Satellite Signal in the Solar Spectrum – Vector (6SV), Remote Sens. Environ., 58, 101–111, 1997.

Vermote, E. F., Tanré, D., Deuzé, J. L., Herman, M., Morcrette, J. J., and Kotchenova, S. Y.: Second simulation of a satellite signal in the solar spectrum – vector (6SV) user guide, version 3, Air Force Res. Lab., Hanscom AFB, MA, USA, 2006a.

Vermote, E. F., and Kotchenova, S.: Atmospheric correction for the monitoring of land surfaces, J. Geophys. Res. Atmos., 113, 2008.

Vermote, E. F., and Saleous, N.: LEDAPS surface reflectance product description, Univ. Maryland, 1–21 pp., 2007.

Vermote, E. F., and Saleous, N.: Operational atmospheric correction of MODIS visible to middle infrared land surface data in the case of an infinite Lambertian target, Earth Sci. Satell. Remote Sens., 1, 123–153, 2006b.

Vermote, E. F., Justice, C., Claverie, M., and Franch, B.: Preliminary analysis of the performance of the Landsat-8/OLI land surface reflectance product, Remote Sens. Environ., 185, 46–56, 2016.

World Meteorological Organization: Report of the expert meeting on aerosols and their climatic effects, WCP-55, Geneva, Switzerland, 1983.

https://doi.org/10.5194/egusphere-2026-1320
Preprint. Discussion started: 7 April 2026

World Meteorological Organization: A preliminary cloudless standard atmosphere for radiation computations, WCP-112, Geneva, Switzerland, 1986.

Zhang, B., Chen, Z., Peng, D., Benediktsson, J. A., Liu, B., Zou, L., Li, J., and Plaza, A.: Remotely sensed big data: evolution in model development for information extraction, Proc. IEEE, 107, 2294–2301, 2019.

Zhang, H., Yan, D., Zhang, B., Fu, Z., Li, B., and Zhang, S.: An operational atmospheric correction framework for multi-source medium-high-resolution remote sensing data of China, Remote Sens., 14, 5590, 2022.